

1 **North American hydroclimate during past warms states: A proxy network-model**
2 **comparison for the Last Interglacial and the mid-Holocene**
3

4 **C. B. de Wet¹, D. E. Ibarra², B. K. Belanger¹, and J. L. Oster¹**

5 ¹Department of Earth and Environmental Sciences, Vanderbilt University, Nashville, TN, USA.

6 ²Earth, Environmental, and Planetary Sciences, Brown University, Providence, RI, USA.

7

8 Corresponding author: Cameron de Wet (Cameron.de.wet@vanderbilt.edu)

9 **Key Points:**

- 10
- 11 • PMIP4 models agree more closely with moisture-sensitive North American proxy
11 networks during the Last Interglacial than the mid-Holocene.
- 12 • A subset ensemble of three models maximizes agreement and suggests SLP gradient
13 differences drove Last Interglacial precipitation patterns.
- 14 • The Last Interglacial may not be a sufficient analog for projected, end-21st century
15 hydroclimatic change in North America.
- 16

17 Abstract

18 During the mid-Holocene (MH: ~6,000 years BP) and Last Interglacial LIG (LIG: ~129,000–
19 116,000 years BP) differences in the seasonal and latitudinal distribution of insolation drove
20 northern hemisphere high-latitude warming comparable to that projected in end-21st century low
21 emissions scenarios, making these intervals potential analogs for future climate change in North
22 America. However, terrestrial precipitation during past warm intervals is not well understood and
23 PMIP4 models produce variable regional moisture patterns in North America during both
24 intervals.

25 To investigate the extent to which the latest generation of models reproduces moisture patterns
26 indicated by proxy records, we compare hydroclimate output from 17 PMIP4 models with
27 networks of moisture-sensitive proxies compiled for North America during the LIG (39 sites)
28 and MH (257 sites). Agreement is lower for the MH, with models producing wet anomalies
29 across the western United States (US) where a high concentration of proxies indicate aridity. The
30 models that agree most closely with the LIG proxies differ from the PMIP4 ensemble by
31 showing relative wetness in the eastern US and dryness in the northwest and central US. An
32 assessment of atmospheric dynamics using an ensemble subset of the three models with the
33 highest agreement suggests that LIG precipitation patterns are driven by weaker winter North
34 Pacific pressure gradients and steeper summer North Pacific and Atlantic gradients. Comparison
35 of this LIG subset ensemble with simulations of future low emissions scenarios indicates that the
36 LIG may not be a sufficient analog for projected, end-21st century hydroclimatic change in
37 North America.

38 Plain Language Summary

39 The mid-Holocene and the Last Interglacial are the two most recent intervals that were warmer
40 than the preindustrial and so are potentially useful analogs for future emissions scenarios. We
41 compare the newest generation of climate models with North American precipitation patterns
42 indicated by proxy records during the MH and LIG. We find that agreement is lower for the MH,
43 with models producing wet anomalies across the western United States (US) where most records
44 indicate drier conditions. Most LIG simulations show wetter conditions than the preindustrial in
45 Alaska, northern Canada, and the southwestern US, yet the models that agree most closely with
46 the LIG proxies also show eastern US wetness and Pacific Northwest and central US aridity.

47 Using a subset of the three models that most closely agree with the LIG proxy records, we find
48 that differences in LIG sea level pressure gradients in the North Pacific and North Atlantic
49 Oceans drove shifts in the spatial and seasonal distribution of precipitation across North
50 America. We observe regional disagreement in precipitation patterns between this LIG subset
51 ensemble and simulations of future emissions scenarios, suggesting that the LIG may not be a
52 sufficient analog for projected, end-21st century hydroclimatic changes in North America.

54 1 Introduction

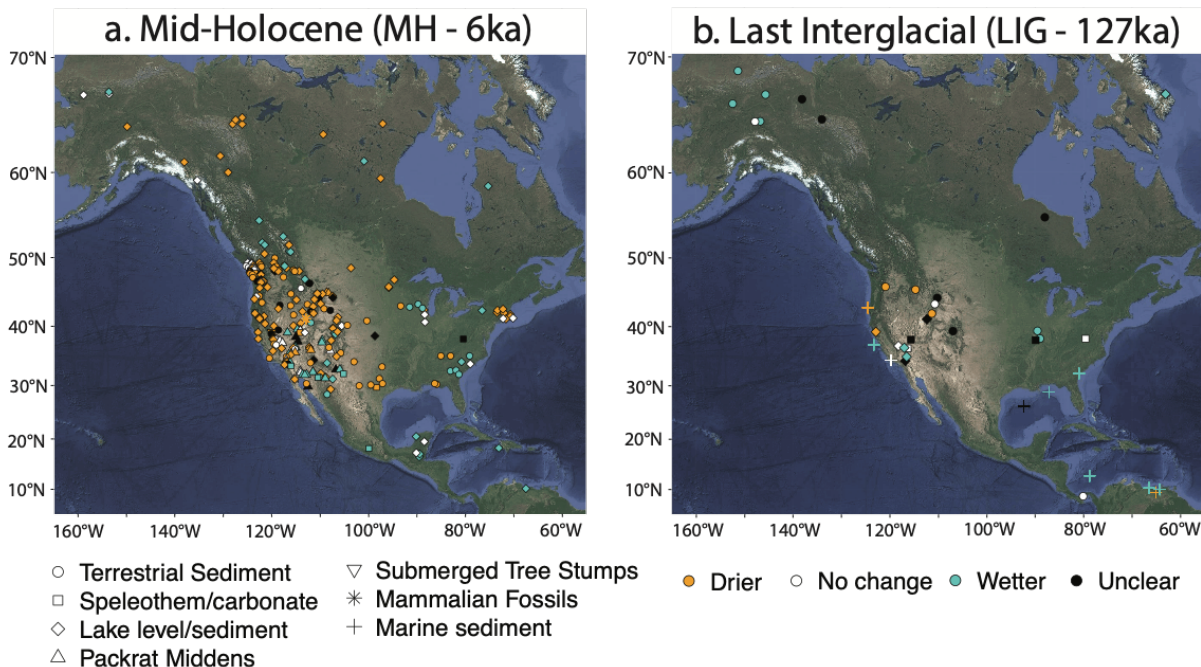
55 Paleoclimate proxy records aggregated for specific intervals in Earth's geologically
56 recent past offer valuable insight into spatiotemporal patterns of hydroclimate change (PAGES
57 Hydro2k Consortium, 2017; Tierney et al., 2020). Comparison of moisture-sensitive proxy
58 networks with paleoclimate model simulations can elucidate the driving mechanisms of past
59 changes in rainfall and effective moisture (e.g., Harrison et al., 2003; Oster et al., 2015; Hermann
60 et al., 2018; Otto-Bliesner et al. 2021; Feng et al. 2022). These comparisons are critical for the

61 assessment of how well the current generation of models reproduce regional hydroclimate
62 patterns suggested by proxy records and can help inform which models may be the most useful
63 for predictions of future moisture availability across hydrologically sensitive regions in a warmer
64 climate state (Tierney et al., 2020). Likewise, comparison of proxy records with climate models
65 can help to refine the interpretations and clarify the biases associated with different proxy types,
66 such as the influence of seasonality or the degree to which different timescales may be resolvable
67 for a reconstructed climate signal (PAGES Hydro2k Consortium 2017).

68
69 The mid-Holocene (MH) (~6,000 years BP) and the Last Interglacial (LIG) period
70 (~129,000–116,000 years BP) are the two most recent intervals with northern hemisphere
71 temperatures comparable to low emissions scenarios for the end of the 21st century (Burke et al.,
72 2018) and may offer glimpses of future hydroclimate in regions like North America. Despite
73 similar greenhouse gas concentrations as the pre-industrial (PI), the MH may have been up to
74 0.7°C warmer than the PI (Marcott et al., 2013). However, recent estimates using data
75 assimilation techniques indicate that global temperatures during the MH may instead have been
76 similar to the PI (Osman et al., 2021). Nonetheless, orbitally driven differences in the seasonal
77 and latitudinal distribution of incoming solar radiation during the MH relative to the modern
78 drove an enhanced seasonal temperature gradient in North America and likely led to
79 strengthened northern hemisphere (NH) monsoons (Otto-Bliesner et al., 2017). Peak global mean
80 LIG surface temperatures (127–125 ka) are estimated to have been ~0.5°C ($\pm 0.3^{\circ}\text{C}$) warmer
81 than those of the PI (Hoffman et al., 2017) with the greatest warming occurring in the mid- and
82 high latitudes (Turney and Jones, 2010). Like the MH, the LIG had greenhouse gas
83 concentrations roughly equivalent to the pre-industrial (Otto-Bliesner et al., 2017), but even
84 larger seasonal differences in the distribution of insolation than those of the MH, which drove a
85 warmer Arctic (Turney and Jones, 2010), smaller ice sheets, and sea level that was ~6–9 meters
86 higher than present (Dutton et al., 2015).

87
88 With the inclusion of both MH and LIG simulations as Tier-1 experiments in the current
89 CMIP6/PMIP4 modeling efforts (Otto-Bliesner et al., 2017), the organization of updated MH
90 and LIG proxy networks for robust comparison with model output is of significant utility for the
91 paleoclimate community, as well as for planners preparing for future warming (Tingstad et al.,
92 2014; Woodhouse et al., 2016). Importantly, regional terrestrial rainfall and moisture balance
93 dynamics during past warm intervals are even less well understood than temperature variations
94 (Scussolini et al., 2019; Otto-Bliesner et al., 2021; Tierney et al. 2020), partially due to the
95 heterogenous geographic response of the water cycle to past global climate forcing (e.g., Greve
96 et al., 2014; Scheff 2018), including in the western United States (Ibarra et al., 2018). Here we
97 present and discuss aggregated networks of hydroclimate-sensitive proxy records for North
98 America (Figure 1), where PMIP4 models produce highly variable regional precipitation patterns
99 during both the MH and LIG. We statistically compare our proxy networks with annual
100 precipitation and runoff output from 17 individual models, as well as model ensembles, for both
101 time slices to investigate the degree to which the latest generation of climate model simulations
102 reproduces the moisture patterns indicated by the proxy record. We then use a subset ensemble
103 of the three models that agree most closely with the LIG proxy record to investigate the role of
104 atmospheric dynamics in driving rainfall patterns during the LIG and to assess the degree to
105 which the LIG may provide a useful analog for North American hydroclimate in projected, end-
106 21st century warming scenarios.

107



108

109 **Figure 1.** Mid-Holocene (a) and Last Interglacial (b) proxy networks for North America designated by the type of
110 archive (symbol) and moisture designation relative to the pre-industrial for the Mid-Holocene and relative to the
111 Holocene/modern for the Last Interglacial (color).

112 2 Methods

113 2.1 Proxy Networks

114 We compiled networks of moisture-sensitive proxy records for the MH (Figure 1a; Table
115 S1) and LIG (Figure 1b; Table S2) respectively from the published literature for North and
116 Central America (5° to 70° , 190° to 310°). Decades of research in the western US have resulted
117 in dense proxy record coverage for this region during the MH, but the coverage is limited across
118 much of Canada, the south-central US, and Central America (Thompson et al., 1993; Bartlein et
119 al., 1998; Hermann et al., 2018). Our MH network includes 257 records, compiling and building
120 on previously published regional networks including Thompson et al (1993) and Hermann et al.
121 (2018) for western North America, Metcalfe et al. (2015) for the south-west US and Mexico,
122 Gavin and Brubaker (2015) and Steinman et al. (2016) for the Pacific Northwest, and Sundqvist
123 et al. (2014) for Canada and Alaska. The MH network includes proxies from lake sediments,
124 packrat middens, speleothems, and pollen records, as well as one record from submerged tree
125 stumps (Lindstrom, 1990) and one of mammal fossils (Grayson, 2000).

126

127 Proxy records for the LIG are sparse and unevenly distributed in North America, with the
128 Western US and Alaska having the best spatial coverage (Scussolini et al., 2019; Otto-Bliesner et
129 al., 2021). This is in large part because the LIG at 129,000 to 116,000 years BP is beyond the
130 limit of radiocarbon dating ($\sim 50,000$ years BP), complicating the development of well-
131 constrained chronologies for paleoclimate archives. Our LIG network for North America
132 includes 39 records, expanding the work of Scussolini et al. (2019), which included 19 records
133 from North America. Our LIG network consists of lake sediments, marine sediments,
134 speleothems, landscape features, and river-cut exposures. We include two marine sediment cores

135 from the southern Caribbean Sea as they are interpreted as representing shifts in the mean ITCZ
 136 position. For the purposes of comparison, we consider the part of the record that the original
 137 authors identify as the warmest part of MIS5 or MIS5e specifically to represent the LIG.
 138

139 For both time periods, we categorize proxy records as drier (D) or wetter (W) conditions
 140 or no change (N) in annual moisture based on the original author's interpretation of the moisture
 141 signal (Table S1, S2). For the MH, our moisture designations are evaluated for the period 6.0 +/-
 142 1.0 ka relative to the pre-industrial. For the LIG, this moisture designation is made relative to the
 143 Holocene/modern record at a given site or within the record. For both intervals, we also include
 144 records for which no moisture signal can be interpreted due either to poorly resolved
 145 chronologies or an original interpretation of the moisture signal as representing non-local
 146 conditions, coding them as inconclusive (Figure 1). In our MH proxy network 53 sites are
 147 identified as wetter, 140 as drier, 38 exhibit no change, and 25 are considered inconclusive. In
 148 our LIG network 16 proxy sites are identified as wetter, 6 as drier, and 7 as no change in
 149 moisture signal, with 10 inconclusive. In sum, our LIG network contains 13 new records that
 150 were not included in the Scussolini et al. (2019) compilation and that are not designated as
 151 inconclusive, increasing the utility of the LIG proxy network for comparison with model output.
 152

153 2.2 Model Output

154 We compare the MH and LIG proxy networks with output of monthly climatologies from
 155 17 PMIP4 climate models of MH (6ka) and LIG (127ka) simulations accessed via the World
 156 Climate Research Programme (<https://esgf-node.llnl.gov/search/cmip6/>) (Table S3). Of the 17
 157 models used, one (CNRM-CM6-1) provides monthly output for the LIG but not the MH and two
 158 (MPI-ESM1-2-LR, MRI-ESM2) provide monthly output for the MH but not the LIG. Simulation
 159 of terrestrial hydroclimate can differ between Earth system models due to differences in model
 160 resolution, land-surface models of water partitioning, albedo representations and energy budget
 161 schemes, as well as complexity in cloud microphysics controlling precipitation rates, large-scale
 162 circulation patterns and orographic precipitation (e.g., Delire et al., 2002; Dai, 2006; Trenberth,
 163 2011; Dalmonech et al., 2015). We calculate annual precipitation percent anomaly by subtracting
 164 annually averaged monthly precipitation (*pr*) output for the pre-industrial (0ka) run from either
 165 the MH (6ka) run or the LIG (127ka) run and the *pr* output for the end of the 21st century (2071-
 166 2100) from two shared socioeconomic pathway (SSP) simulations (SSP2-4.5 and 5-8.5) from the
 167 historical (1850-1949) simulation in the native model resolution. We calculate annual percent
 168 runoff anomaly by subtracting annually averaged monthly evapotranspiration output (*evspbsl*)
 169 from the annually averaged monthly *pr* output for the LIG and MH relative to the pre-industrial
 170 (e.g., Oster et al., 2015; Hermann et al., 2018; Ibarra et al., 2018). In addition to comparisons
 171 between the proxy networks and annually averaged precipitation and runoff anomalies, we
 172 compare the proxy data with average precipitation and runoff percent anomalies for the winter
 173 half-year (NDJFMA) and summer half-year (MJJASO).
 174

175 2.3 Agreement Coefficients

176 We compare hydroclimate changes simulated by each model at each proxy site with the
 177 change observed in the proxy networks by using the Gwet's AC2 statistic (Eq. 1) for categorical
 178 agreement between two raters (proxies and models) which classify items (sites) into categories
 179 (wetter, drier, no change) relative to the probability of random chance agreement (Gwet, 2008;
 180 Gwet, 2015; Conroy et al., 2019; Feng et al., 2022). The AC2 statistic is given by

181

$$(Eq. 1) AC2 = Pa - Pe_1 - Pe$$

183

184 Where P_a is the percentage of agreement between the proxies and the model output and P_e
 185 is the expected percentage of agreement between the two due to chance alone. If models and
 186 proxy data are in complete agreement, then the AC2 agreement coefficient will be equal to 1. If
 187 there is no agreement between the two beyond what is expected by random chance, then the AC2
 188 will be equal to 0. Opposite agreement between the models and proxy data (i.e., the model
 189 indicates wetter conditions at every site where the proxies suggest drier and vice versa) would be
 190 represented by an AC2 of -1. The Gwet's AC2 statistic weights observations based on the degree
 191 of model-proxy agreement by multiplying a matrix of the model-proxy observations by a weight
 192 matrix in which strong agreement (e.g., both the model and proxy indicate wetter conditions at a
 193 particular site) is given a weight of 1, strong disagreement (e.g., the model indicates drier
 194 conditions, the proxy indicates wetter) is given a weight of 0, and weak disagreement (e.g., the
 195 model indicates drier, the proxy indicates no change) is given a weight of 0.5. To identify
 196 maximum possible agreement between each model and the proxy networks we vary the threshold
 197 value for a change in pr or runoff to be considered wetter or drier from 1 to 20% in 1%
 198 increments. For example, at a threshold of 10%, a model must simulate MH precipitation \geq
 199 110% of the PI for a site to be classified as wetter and \leq 90% of the PI to be classified as drier.
 200 We chose a maximum rainfall threshold of 20% because this value encompasses the range of
 201 average relative standard deviations of simulated pre-industrial annual precipitation for North
 202 American grid cells from each model.

203

204 For comparison, we also present the Gwet's AC1 and the weighted Cohen's kappa (K_w)
 205 statistic, which has been used by similar proxy network-model comparison studies (e.g., DiNezio
 206 and Tierney, 2013; Oster et al., 2015; Oster and Ibarra, 2019), including for the MH (Hermann et
 207 al. 2018). K_w weights observations based on the degree of model-proxy disagreement, allowing
 208 for the presence of weak disagreement to positively influence the statistic in a similar fashion to
 209 Gwet's AC2. Gwet's AC1 is the first-order version of Gwet's AC2 and does not weight
 210 observations. That is, weak disagreement is considered mathematically identical to strong
 211 disagreement. Our calculated AC2 values tend to be higher than both K_w and AC1. We focus our
 212 discussion on our AC2 calculations because it takes weak disagreement into account, which AC1
 213 does not. Additionally, AC2 is understood to be a more reliable metric than K_w for the degree of
 214 agreement between rates in the presence of high agreement and high prevalence of one category
 215 (e.g. Wongpakaran et al., 2013; Gwet, 2015).

216

217 3 Results

218 3.1 Mid-Holocene proxy network observations

219 The moisture patterns shown by our updated MH proxy network ($n = 188$ records in
 220 western North America) are largely consistent with observations from Hermann et al. (2018) ($n =$
 221 170 records) and Thompson et al. (1993) ($n = 99$) for western North America. The western US,
 222 where moisture patterns are dominated by winter westerly storm-sourced rainfall, is
 223 characterized by increased aridity during the MH relative to the PI. As in Hermann et al. (2018),
 224 central and northern California, the Pacific Northwest, and the northern Rocky Mountain regions
 225 are consistently drier than the modern, while the Great Basin and southern Rockies exhibit both

wet and dry sites and sites with no change (Figure 1a). Areas in the southwestern US and northern Mexico where the North American Monsoon contributes significantly to annual rainfall show a mixed response. Most sites along the US-Mexico border indicate increased MH wetness, whereas sites from northern New Mexico and northern Arizona suggest enhanced aridity.

230

We expand on the geographical range of the network from Hermann et al. (2018) (25°N to 55°N , 100°W to 130°W) by including proxy archives from across North America (5°N to 70°N , 190°W to 310°W), though the proxy coverage is more sparse outside of the western US due to taphonomy and preservation bias favoring arid regions versus wetter regions (Figure 1a). Modern precipitation patterns become less seasonal east of the Rocky Mountain and western Great Plains regions, with a roughly equal distribution of summer and winter moisture (Lora and Ibarra, 2019; Schneider et al., 2011; PRISM Climate Group, 2010). Archives from the Plains region in Texas and the Florida Panhandle demonstrate aridity ($n = 8$), as do several archives from southern New England ($n = 10$). Meanwhile, archives from the Carolinas and coastal Georgia indicate greater wetness during the MH ($n = 6$). A collection of sites in the upper Midwest shows a mixed response ($n = 9$). All the sites that we include from the Yucatan Peninsula, Central America, and the Caribbean region indicate wetter conditions or no change ($n = 9$). In Canada, southern British Columbia was drier along the border with the US ($n = 5$), with wetter conditions further north ($n = 5$). Drier conditions are observable in the Yukon and the Northwest Territories, and southern Nunavut ($n = 12$), aside from one wetter site in central Canada. Sites from Alaska display a mixed response with two showing no change, one wetter, and one drier ($n = 4$).

248

MH - PI Annual Rainfall

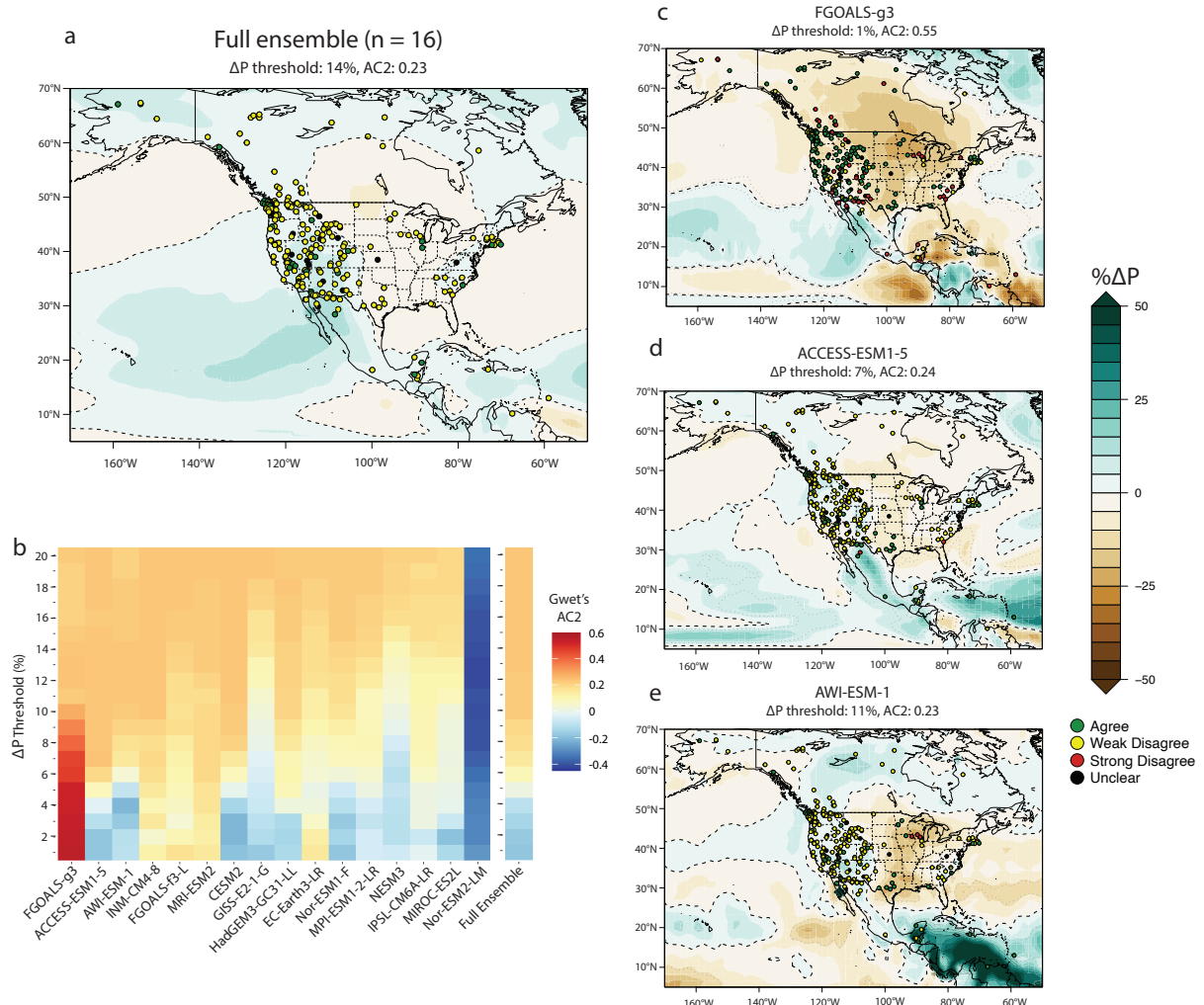


Figure 2. (a) Annual MH-PI precipitation anomaly (% ΔP) for the full PMIP4 ensemble ($n=16$) with MH proxy network plotted based on agreement with the ensemble climatology. (b) Heat map showing AC2 values at each threshold (1-20%) for the MH-PI annual precipitation anomaly to be considered wetter, drier, or unchanged. (c - d) Annual MH-PI precipitation anomaly (% ΔP) with MH proxy network plotted based on agreement with the underlying model climatology for three representative models (c: FGOALS-g3, d: ACCESS-ESM1-5, e: AWI-ESM-1). Dark gray dashed lines denote the boundary between positive and negative precipitation anomalies. Light gray dotted lines denote the threshold for the change in precipitation to be considered wetter, drier, or unchanged based on optimized agreement with the proxy network.

3.2 Mid-Holocene proxy network – model comparisons

Overall, agreement between the MH proxy network and model simulations is low for both annual precipitation (Figure 2b, Figure S1) and runoff (Figure S1). The full PMIP4 MH ensemble produces an AC2 value of 0.23 at a rainfall threshold of 13% (Figure 2a). Fourteen of the 16 models that provide MH output produce AC2 agreement coefficients between 0.19 and 0.24, with optimized rainfall thresholds that range from 7% to our maximum allowable value of 20%, and nine of the 16 models optimized at a threshold of 16% or higher (Figure 2b). These simulations show wetter MH conditions relative to the modern along the western US-Mexico border, where proxies also indicate enhanced wetness. However, most models also show some

268 pattern of enhanced wetness over all or part of California, the Great Basin, the Pacific Northwest,
 269 and the Colorado Plateau, where a high concentration of archives generally indicate enhanced
 270 MH aridity. Since the wet anomaly in the simulations tends to be relatively modest (generally
 271 less than 20% wetter than the PI) our algorithm maximizes agreement by increasing the rainfall
 272 threshold such that most western US dry sites are categorized as weakly disagreeing with the
 273 lack of significant hydroclimate change in most of the simulations. Thus, the MH simulations for
 274 which agreement in the western US is optimized by increasing the precipitation threshold also
 275 tend to produce weak disagreement with wetter or drier archives across other regions in North
 276 America where modeled changes are small, such as the eastern US and Great Plains. ACCESS-
 277 ESM1-5 (Figure 2d) and AWI-ESM-1 (Figure 2e) are exceptions in that they produce the second
 278 and third highest AC2 and are optimized at relatively lower threshold values of 7% and 11%
 279 respectively. However, agreement for ACCESS-ESM1-5 and AWI-ESM-1 is only marginally
 280 higher than most of the other models for which all or most locations are characterized as ‘no
 281 change’. One model, Nor-ESM2-LM, produces a large wet anomaly along the western coast of
 282 Canada that extends down into the western US, driving widespread disagreement with the proxy
 283 network and negative AC2 value that is not considered statistically significant ($p = 2$) (Figure
 284 S1).

285
 286 FGOALS-g3 stands out in our MH comparisons with an AC2 value of 0.55 at a rainfall
 287 threshold of 1% and 0.52 or higher at a threshold of 5% or less (Figure 2c). This is driven by
 288 widespread aridity across most of the US and Canada and thus good agreement with the large
 289 concentration of “drier” proxy sites in the western US. Additionally, FGOALS-g3 produces wet
 290 anomalies in southern California and southwestern Arizona, driving good agreement with the
 291 wetter archives along the western portion of the US – Mexico border. However, this wet
 292 anomaly in the simulation does not extend east to the numerous wet sites in southeastern
 293 Arizona, northern Mexico, and southern New Mexico. Indeed, the rest of the US and most of
 294 Canada are characterized by aridity, driving agreement with concentrations of drier proxy sites in
 295 Texas, the northeast, and parts of the Midwest, as well as northwest Canada, but disagreement
 296 with the enhanced wetness of the Yucatán Peninsula, southeast US, and southern Wisconsin
 297 sites.

298
 299 Kw values are lower than AC2 values for all models, ranging from 0.19 to -0.044, and are
 300 identified as not statistically significant for eight of the 16 models analyzed. AC1 values are also
 301 lower than AC2 values for all MH simulations, ranging from 0.51 to -0.09. Our calculated AC1
 302 values for 11 of the 16 MH simulations are identified as not significant ($p > 0.05$) (Table S3).
 303 Thus, we focus on the MH AC2 values in our discussion.

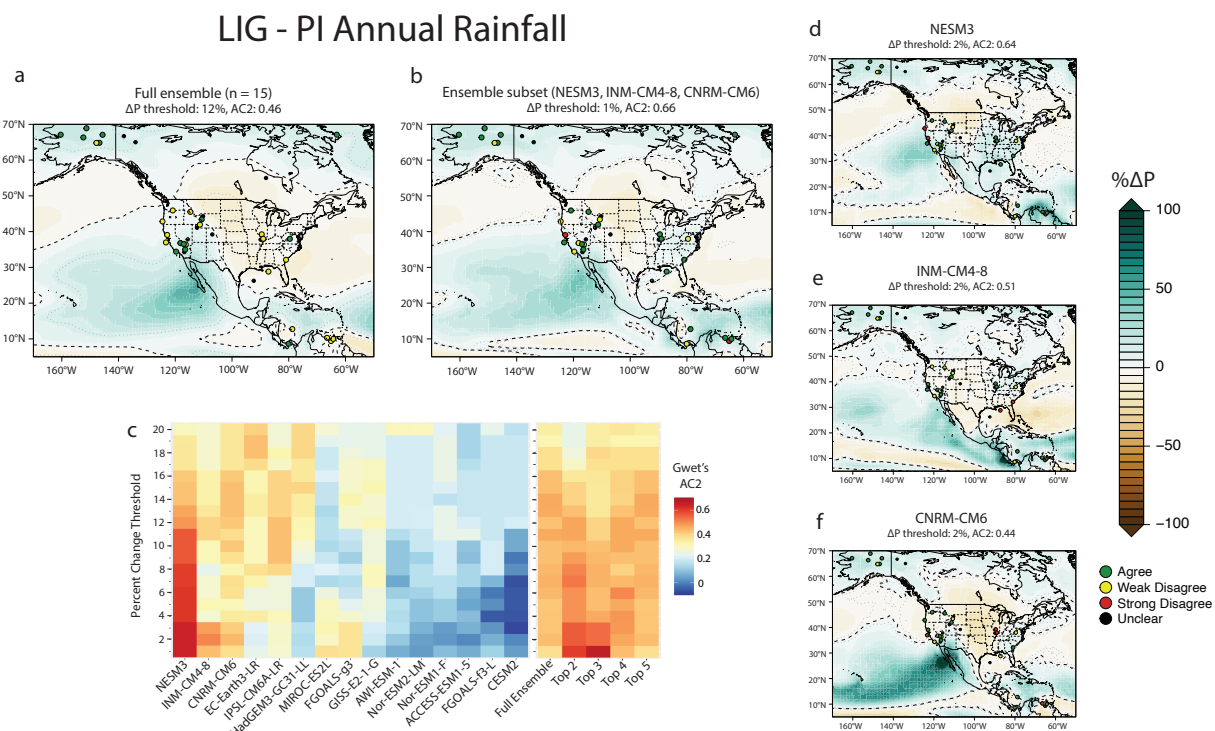
304
 305 3.3 Last Interglacial proxy network observations
 306 LIG proxy records from the western US document drier conditions across the Pacific
 307 Northwest and northern Rockies and increased wetness in the southwest (Figure 1b; Table S2
 308 and references therein). Marine sediment cores, the chronologies for which are tuned to
 309 SPECMAP (Pisias et al., 1984), indicate drier conditions along the Oregon coast and wetter
 310 conditions or conditions similar to today along the California coast (Pisias et al., 2001; Heusser
 311 et al., 2000; Lyle et al., 2010). The chronologies for the various western US lake records are also
 312 largely controlled by correlations to SPECMAP due to being well beyond the effective dating
 313 range for radiocarbon. These records track vegetation changes and shifts in lake water levels,

314 with lakes from the northern US Rockies (Jiménez-Moreno et al., 2007), the Pacific Northwest
315 (Whitlock and Bartlein, 1997), and northern California (Adam and West, 1983) indicating
316 relative aridity during the LIG, while Great Basin lakes document wetter conditions or conditions
317 similar to the present (Rehies et al., 2012; Forester et al., 2005; Woolfenden, 2003). Other lake
318 records from the Yellowstone area (Baker, 1986), the Colorado Rockies (Anderson et al., 2014;
319 Miller et al., 2014; Sharpe and Bright, 2014), northern Utah (Balch et al., 2005), and southern
320 California (Glover et al., 2017) do not display clear signals of LIG hydroclimate.
321

322 Much of the existing literature for MIS5e climate conditions in Alaska focuses on
323 temperature reconstructions as opposed to moisture conditions. However, it is hypothesized that
324 warmer temperatures during the LIG drove wetter conditions across Alaska by increasing
325 atmospheric water vapor content and accelerating the regional hydrologic cycle, as well as by
326 decreasing the proportion of precipitation that fell as snowfall during shortened Arctic winters
327 (CAPE Last Interglacial Project Members, 2006; Miller et al., 2010). We identify four Alaskan
328 proxy sites across the central and northern portions of the state that indicate wetter LIG
329 conditions based on pollen assemblages in lake cores (Muhs et al., 2001; CAPE Last Interglacial
330 Project Members, 2006; Bigelow et al., 2014), river cut exposures (Bigelow et al., 2014), or
331 paleosol data, as well as one soil record that indicates no change in moisture (Pewe et al., 1997).
332 We also identify two sites, a record of soil formation (Tarnocai, 1990) and of pollen, plant
333 fossils, and insect remains from a river bluff (Schweger and Matthews, 1991), that suggest
334 warmer, but not necessarily wetter conditions in the Yukon region of western Canada. There are
335 relatively few LIG records available for the rest of mainland Canada, likely due to the erosive
336 nature of the Laurentide ice sheet during the last glaciation (LIGA Members, 1991). We identify
337 one record of amino acids, pollen, and microfossils in buried organic sediments from the Hudson
338 Bay lowlands that is suitable for inclusion in our network based on the continuous chronology,
339 but which displays an uncertain climate signal at the LIG (Wyatt, 1990; LIGA Members, 1991).
340

341 Of the few LIG proxy records that exist from the eastern US, the majority indicate
342 increased moisture. However, the poor proxy record coverage limits our ability to make broad-
343 scale interpretations of hydroclimate changes for this region. Pollen records from two southern
344 Illinoisan lakes document shifts to more temperate deciduous forests during the LIG and have
345 been interpreted as indicative of wetter conditions relative to the present (Teed, 2000; Curry and
346 Baker, 2000). Alkenes, $\delta^{13}\text{C}$, and $\delta^{18}\text{O}$ in plant leaf waxes in a northern Gulf of Mexico marine
347 sediment core and terrestrial pollen fluctuations in a core off the coast of South Carolina and
348 Georgia indicate that wetter than modern conditions persisted in the southeastern US during the
349 LIG (Limoges et al., 2014; Suh et al., 2019). Changes in geochemistry and mineralogy in marine
350 sediment core MD02-2549 from the north central Gulf of Mexico suggest changes in sediment
351 provenance and relative contributions from different sub-basins, indicating a northeast migration
352 of the main rainfall belt over the Mississippi River basin in response to greater boreal summer
353 insolation of the LIG (Montero-Sessano et al. 2011). While this hypothesis is consistent with the
354 increased wetness observable in Illinoisan lakes (Teed, 2000; Curry and Baker, 2000), we opt to
355 code this core site as unclear in our proxy network because the signal interpreted by Montero-
356 Serrano et al. (2011) is highly non-local. Additionally, two LIG speleothem records show no
357 change in moisture conditions in western Virginia (Springer et al., 2014) and an inconclusive
358 moisture signal in southeastern Missouri (Knight et al. 2006).
359

360 We identify one Central American soil record and two Caribbean Sea marine sediment
 361 cores that meet our criteria for inclusion in the LIG network. Pollen data from the U/Th-dated
 362 soil record of El Valle, Panama is indicative of hydroclimate conditions similar to that of today
 363 (Cárdenes-Sandí et al., 2019), while Mg/Ca and $\delta^{18}\text{O}$ data from the proximal SPECMAP-tuned
 364 ODP Core 999A have been interpreted as indicating lower sea surface salinity than the present
 365 and wetter conditions at the LIG (Schmidt and Spero, 2011), though Scussolini et al. (2019) note
 366 that the signal is weak and uncertainty is large in the record. Ribolleau et al. (2014) interpret
 367 sedimentological variations in a Cariaco Basin core to indicate less rainfall over the Unare river
 368 basin and more rainfall over the Tuy and Neveri river basins during the LIG. The authors argue
 369 the LIG preference for enhanced rainfall over the more northern Tuy and Neveri Basins indicates
 370 a northern shift of the ITCZ and rain belts compared to the Holocene (Ribolleau et al. 2014).
 371 Here we adopt the approximate locations of the river basins from Scussolini et al. (2019) for the
 372 purpose of plotting the sign of change at the sites.
 373



374
 375 **Figure 3.** (a) Annual LIG-PI precipitation anomaly (% ΔP) for the full PMIP4 ensemble ($n=15$) with LIG proxy
 376 network plotted based on agreement with the ensemble climatology. (b) Annual LIG-PI precipitation anomaly
 377 (% ΔP) for the full ensemble subset of the three models that agree most closely with the LIG proxy network. (c) Heat
 378 map same as in Figure 2 for LIG-PI, including AC2 values for the full PMIP4 ensemble and ensembles of the top
 379 two, three, four, and five models in terms of agreement with the LIG proxy network. (d - f) Same as Figure 2 for
 380 three models in the ensemble in b. (d: NESM3, e: INM-CM4-8, f: CNRM-CM6). Dark gray dashed and light gray
 381 dotted lines same as in Figure 2.

382
 383 **3.4 Last Interglacial proxy network – model comparisons**
 384 Agreement between the proxy network and model simulations is greater for the LIG than
 385 for the MH for both precipitation (Figure 3c) and effective moisture (Supplement XX). The LIG
 386 ensemble ($n = 15$) produces an AC2 value of 0.46 at an intermediate rainfall threshold of 12%
 387 (Figure 3a), which is a higher degree of agreement than 13 of the 15 individual models (Figure

388 3c). The model NESM3 produces the highest degree of agreement with the proxy network, with
 389 an AC2 value of 0.64 at a rainfall threshold of 1, 2, or 3% (Figure 3d). The models INM-CM4-8
 390 (Figure 3e) and CNRM-CM6 (Figure 3f) display the second and third highest values, 0.51 and
 391 0.44 respectively, at rainfall thresholds of 2%. Most other models are optimized at rainfall
 392 thresholds between 12% and 20% and display AC2 values that range from 0.21 to 0.43 (Figure
 393 3c). MIROC-ES2L and FGOALS-g3 are the only two models with middling AC2 values (0.38
 394 and 0.37 respectively) that are optimized at rainfall thresholds of less than 2%. The four models
 395 with AC2 values of less than 0.25 are not considered statistically significant comparisons ($p >$
 396 0.05).

397

398 Increased rainfall in Alaska and the southwest US, where LIG proxies indicate wetter
 399 conditions, is relatively consistent across all models and is represented by robust wetness (>12%
 400 rainfall anomaly) in the ensemble (Figure 3). Most models and the ensemble also show a domain
 401 of increased LIG aridity in the northern Great Plains, though there are no LIG proxy sites in this
 402 region for comparison. There is significant disagreement in the sign of rainfall change between
 403 models across most of the rest of North America, though the magnitude of anomaly tends to be
 404 smaller than in the southwest US or northern Great Plains. The LIG ensemble is characterized by
 405 a transition between wetness in the west and aridity in the Midwest and east that runs from
 406 southeastern New Mexico through Idaho, though the magnitude of anomaly across these regions
 407 is below the optimized rainfall threshold of 12%. This pattern drives weak disagreement with the
 408 drier proxy records distributed across the Pacific Northwest and Rocky Mountain region and
 409 with the wetter records of southern Illinois, the Gulf of Mexico, and the coastal southeast US.

410

411 K_w values are lower than AC2 values for all LIG simulations, as are AC1 values, though
 412 to a lesser degree. The same four models perform the best across all three metrics except for
 413 FGOALS-g3, which improves from eighth highest AC2 to second highest K_w and fourth highest
 414 AC1. K_w values less than 0.2 (10 models) and AC1 values less than 0.22 (9 models) are
 415 statistically nonsignificant results ($p > 0.05$) (Table S4). As with the MH, we focus our
 416 discussion on LIG AC2 values.

417

418 4 Discussion

419 4.1 Mid-Holocene comparisons and climate interpretations

420 Our findings are consistent with previous analyses of PMIP simulations which found that
 421 models produce opposite sign and/or smaller magnitude MH precipitation anomalies in North
 422 America than are suggested by paleoclimate proxy reconstructions (Braconnot et al., 2012;
 423 Harrison et al., 2015, 2016; Hermann et al., 2018). Like Hermann et al. (2018), overall
 424 agreement between the expanded North American proxy network and MH simulations is low and
 425 FGOALS-g3 displays the highest degree of agreement. This agreement appears to be largely
 426 driven by widespread MH dry anomalies in western North America present in both FGOALS-g2
 427 (Hermann et al., 2018) and FGOALS-g3 (this study) simulations, where there is a high
 428 concentration of proxies that indicate aridity.

429

430 The fact that the calculated AC2 values for our new expanded proxy network (Table S3)
 431 and for the western US proxy network from Hermann et al. (2018) (Table S5) tend to be higher
 432 overall than the K_w values from Hermann et al. (2018) is likely because K_w may be an unreliable

metric in cases where agreement is high and there is a large prevalence of one category (Wongparakan et al., 2013; Gwet, 2008; Gwet, 2015). This is the case for comparisons between model simulations and the MH proxy network, which is skewed toward drier conditions and likely explains why the K_w values for the expanded MH proxy network of this study are lower than the AC2 values. Thus, we identify Gwet's AC2 as a more reliable metric for comparisons between climate model output and categorical proxy data and recommend its use for these types of analyses (cf. Feng et al., 2022). However, we do not interpret our higher AC2 values for the expanded network relative to the K_w values for the western US from Hermann et al. (2018) as necessarily indicative of a meaningful improvement on proxy network-model agreement for the MH since this finding is at least partly an artifact of the metrics themselves.

443

In most cases, our algorithm for choosing a MH precipitation threshold to optimize AC2 results in large thresholds, widespread weak disagreement with any proxy site that is coded as wetter or drier, and a clustering of AC2 values between 0.19 and 0.23. This makes it difficult to differentiate between models in terms of agreement with our expanded proxy network, despite considerable variability in the pattern of precipitation anomalies across North America between model simulations. It is possible that MH proxies are responding in a non-linear way, recording signals of increased aridity in response to small changes in actual rainfall, or are being interpreted here and in past literature as annual signals when they are in fact biased toward anomalies present only in particular seasons.

453

Alternatively, the MH hydroclimate patterns suggested by the proxy network may be largely driven by climate feedbacks, such as vegetation shifts, that are not fully represented in the model simulations. Changes in vegetation can influence climate via changes to water cycling, surface albedo, and dust mobilization (Thompson et al., 2022) and can drive different dynamical circulation patterns than those expected from orbital, greenhouse gas, and ice sheet forcing alone (Swann et al. 2014). Since the differences in orbital forcing and other CMIP6/PMIP4 boundary conditions between the MH and PI are relatively small, especially compared to those of the LIG, these finer-scale emergent climate feedbacks, such as vegetation response to seasonally biased MH warming, may be especially important for the precipitation dynamics of the MH. None of the MH simulations include fully dynamic vegetation and the few that include interactive vegetation do not stand out in the quality of comparison with the MH proxy network (Table S3). Recent modeling efforts with varying prescriptions for vegetation in the African Sahara, NH mid-latitudes, and Arctic have yielded improved agreement with temperature estimates from the Temperature12K database (Kaufman et al., 2020) during the Holocene (Thompson et al. 2022). Further, vegetation feedbacks during the MH such as a Green Sahara (Tabor et al. 2020) or expanded Eurasian forest cover (Swann et al. 2014) have been shown to help resolve mismatches between simulated and observed precipitation response on a global scale. While dynamical treatment of vegetation remains a challenge for Earth system models of past and present climates, it may contribute to the mismatch between our North American proxy network and the CMIP6/PMIP4 simulations. Additionally, despite the higher resolution of the CMIP6/PMIP4 simulations, they appear not to have improved in terms of the simulation of extratropical circulation relative to CMIP5/PMIP3 (Brierley et al., 2019), an issue that has been pinpointed as a likely cause of mismatches between simulated and observed moisture patterns in Eurasia (Bartlein et al., 2017) and Europe (Mauri et al., 2014) and one that may play an important role for North America as well. The persistent mismatch between the modest MH rainfall anomalies

478

479 of PMIP simulations and the patterns evident in MH proxy networks deserves further
480 consideration.

481

482 4.2 Last Interglacial comparisons and climate interpretations

483 Our LIG analyses expand upon previous work by Scussolini et al. (2019), whose
484 comparisons show agreement between their proxy network and model ensemble ($n = 7$) on
485 increased LIG rainfall in Alaska and northern South America, but an ambiguous relationship
486 across the contiguous US. Similarly, we observe weak disagreement between our LIG ensemble
487 ($n = 15$) and expanded LIG proxy network in much of the US (Figure 3a).

488 We find that an ensemble of the three models that most closely agree with the LIG proxy
489 network and are optimized at a relatively low rainfall threshold of 2% – NESM3, INM-CM4-8,
490 and CNRM-CM6 – maximizes agreement with the LIG proxy network relative to any other
491 individual model or combination of models (Figure 3b). This subset ensemble displays an AC2
492 value of 0.66 at an optimized rainfall threshold of 1%. Agreement with the wetter proxy sites in
493 Alaska and southern California is consistent between the subset ensemble ($n = 3$) and full
494 ensemble ($n = 15$). However, the subset ensemble shows better agreement with drier proxy sites
495 in the Pacific Northwest and in the Rocky Mountains, where it displays low magnitude, but
496 robust dry anomalies. The low magnitude wet anomalies in the full ensemble are below the
497 optimized rainfall threshold, driving weak disagreement with all but the Porcupine Creek record
498 of western Wyoming which has been interpreted as representing moisture conditions similar to
499 the present day (Pierce et al., 2011). The subset also aligns more closely with the wetter proxy
500 sites of southern Illinois in the Midwest US and of the Gulf of Mexico and the coastal southeast
501 US, all of which are situated close to the wet-dry anomaly transition, likely contributing to the
502 low optimized rainfall threshold of the subset ensemble. Thus, our subset ensemble may help
503 reconcile disagreement between the aridity in the Mississippi River Basin of the full LIG
504 ensemble and LIG proxies in southern Illinois, which indicate enhanced LIG rainfall. Finally, the
505 subset shows a wetter southern Caribbean, where three of the five records in our compilation are
506 wetter, compared to the ambiguous climatology of the full ensemble.

506

507 4.3 Last Interglacial seasonal considerations

508 Individual PMIP4 simulations display variable responses to the enhanced seasonality that
509 was driven by the orbital forcing of the LIG. We avoid quantitative comparisons between models
510 and proxies on a seasonal basis because robust seasonal biases in LIG proxy records are often
511 unclear, speculative, or in development in the paleoclimate proxy literature (Kwiacienski et al.,
512 2022 and references therein). Instead, we compare the subset of models that maximize annual
513 agreement with the LIG proxy network (Figure 4c, d) with the full PMIP4 ensemble (Figure 4a,
514 b) to help elucidate some of the seasonal patterns in North American LIG rainfall. During the
515 LIG summer half-year (MJJASO) both the full ensemble and the ensemble subset are
516 characterized by wetter conditions across Alaska, northern Canada, and Mexico and drier
517 conditions in southern Canada, the central US, and the Pacific Northwest (Figure 4a, c). Both
518 show enhanced aridity in eastern Canada, the northern Great Plains, and northeast US and wetter
519 conditions in the southwestern US and Mexico during the winter half-year (NDJFMA) (Figure
520 4b, d).

521

522

524 During the winter half-year (NDJFMA) the subset ensemble shows increased rainfall in
525 the southeastern US, where the full ensemble indicates aridity, and a mix of wet and dry
526 conditions along the northwest coast of the US and Canada, where the full ensemble shows
527 contiguous wetness (Figure 4b, d). The subset ensemble displays more widespread wet
528 conditions in the eastern US and in northern South America during the summer half-year relative
529 to the full ensemble (Figure 4a, c).

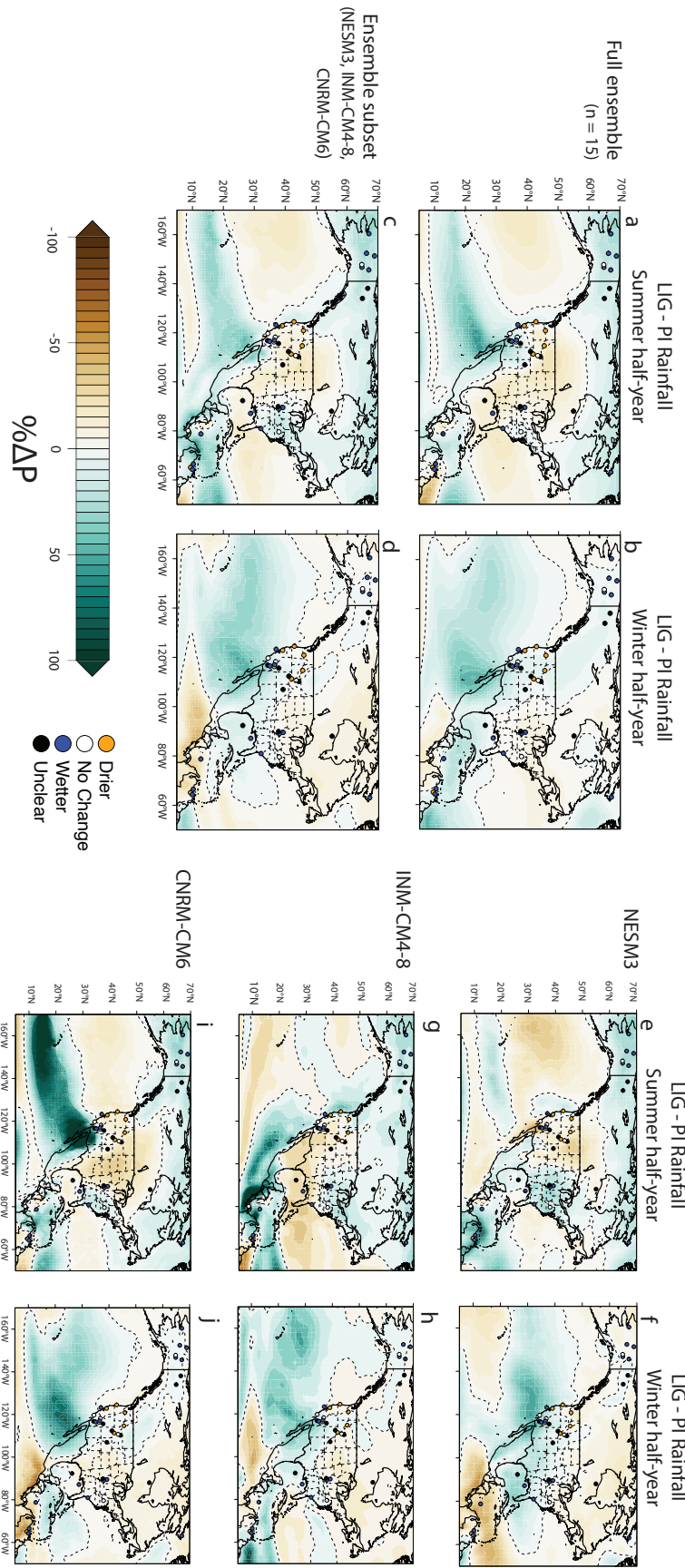
530

531 Additionally, the subset ensemble differs from the full ensemble in terms of the seasonal
532 pattern of wet anomalies in the North American Monsoon (NAM) region. While many models
533 show a positive annual rainfall anomaly in the southwestern US, a closer look at the spatial
534 distribution and seasonal balance of rainfall between models indicates that different mechanisms
535 drive this annual anomaly in each model (Figure 4). The annual increase in rainfall in the
536 southern US may result from an expanded and strengthened NAM, a strengthened, but not
537 significantly expanded monsoon, or an increase in southwesterly winter rainfall. Scussolini et al.
538 (2019) observe a wetter and somewhat spatially expanded LIG NAM in their ensemble
539 climatology, though there is considerable inter-model spread that hinders a more conclusive
540 understanding of how far into California and/or the Great Basin this anomaly extends. Similarly,
541 our full ensemble shows enhanced summer half-year rainfall occurring from southern California
542 into the southern Great Basin and as far east as central New Mexico (Figure 4a). The subset
543 ensemble differs from the full ensemble in that it is characterized by a summer half-year rainfall
544 anomaly that extends northward from Mexico but is localized to Arizona within the United
545 States and does not extend west to the wetter LIG proxies of southern California (Figure 4c).
546 Taken individually, there is disagreement among the top three models in the spatial distribution
547 of summer moisture in the southwestern United States. NESM3 shows enhanced rainfall across
548 Mexico and into Arizona and New Mexico (Figure 4e). INM-CM4-8 displays an opposite
549 response, showing enhanced summer aridity across the NAM domain, including northern and
550 central Mexico (Figure 4g). CNRM-CM6 shows greatly enhanced rainfall in southern California
551 and Arizona that extends northward into southern Nevada (Figure 4i). A lack of resolvable
552 proxies in northern Mexico, Arizona, and New Mexico, as well as the southern Rockies, makes
553 specific interpretations about the geometry of the NAM domain during the LIG challenging. The
554 development of new proxy records from these climatologically important but currently
555 unrepresented locations will be key for generating a better understanding of the characteristics of
556 regional precipitation patterns during the LIG, like the NAM.

557

558 The top three models are in much closer agreement with regard to cool season rainfall,
559 with all three showing enhanced wetness across the southwest US during the winter half-year
560 (Figure 4f, h, j). Thus, a key finding of this work is that this subset of models indicates that the
561 NAM may have been strengthened, but perhaps not significantly expanded during the LIG and
562 that the enhanced annual wetness of the southwestern US, including that which is demonstrated
563 by the southern California proxies, was driven primarily by increased southwesterly wintertime
564 rainfall not summertime monsoonal rainfall.

565



567 **Figure 4.** Summer (MJASO) and winter (NDJFMA) half-year LIG - PI rainfall anomalies for the full PMIP4
568 ensemble (a and b), the ensemble subset (c and d), and the three models that make up the ensemble subset (NESM3:
569 e and f; INM-CM4-8: g and h; CNRM-CM6: i and j). Proxy sites are plotted based on rainfall designation at the LIG
570 relative to the PI. Dark gray dashed lines and light gray dotted lines same as in Figure 2.
571

572 4.4 Atmospheric dynamics during the Last Interglacial

573 To assess the atmospheric drivers of LIG moisture patterns, we present sea level pressure
574 (SLP) and 850 hPa wind vector output for the ensemble of the three models that agree most
575 closely with the LIG proxy record (Figure 5). Interactions between the semi-permanent pressure
576 systems over the Pacific and Atlantic play a large role in the amount and seasonal distribution of
577 rainfall that falls across much of North America (e.g., Wise, 2016). Specifically, the location and
578 relative strength of the North Pacific High (NPH) and Aleutian Low (AL) are relevant for the
579 geometry of winter storm tracks that deliver moisture to Alaska and the western US, where there
580 is a large concentration of LIG proxy sites (e.g., Oster et al., 2015; Wong et al., 2016; Swain,
581 2015). In the eastern US, the gradient between low SLP in the subtropical Atlantic Ocean and
582 high SLP in the north Atlantic and the position of the North Atlantic Subtropical High (NASH)
583 and has been shown to play a large role in the amount and source of rainfall during both the
584 modern (Labosier and Quiring, 2013; Diem, 2012; Li et al., 2011) and the Holocene (Hardt et al.,
585 2010), including via the incidence of summer tropical cyclones along the Gulf Coast and east
586 coast of North America (e.g., Baldini et al., 2016). An assessment of how these pressure systems
587 differed under the enhanced seasonality of the LIG relative to the PI may thus provide insights
588 into the mechanisms driving the spatial patterns and seasonal distribution of LIG rainfall.
589

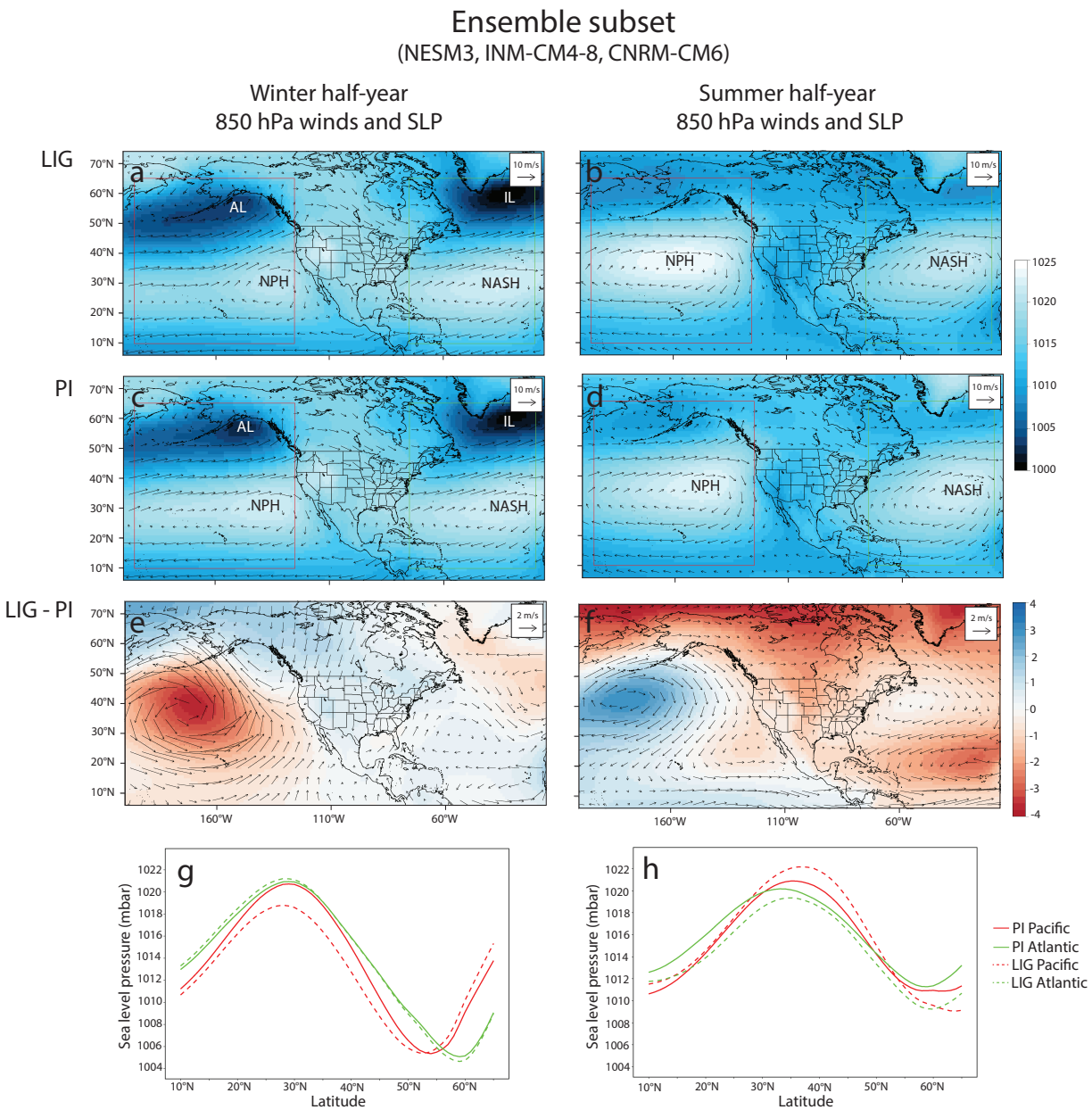


Figure 5. Ensemble subset summer half-year and winter half-year 850 hPa wind vectors and sea level pressure for the LIG (a, b), PI (c, d), and LIG-PI anomaly (e, f). Latitudinal pressure gradient for 10°N to 65°N zonally averaged from 165°W to 235°W in the Pacific Ocean (red box in a-d) and from 75°W to 20°W in the Atlantic Ocean (green box in a-d) for the LIG and PI. AL: Aleutian Low. NPH: North Pacific High. IL: Icelandic Low. NASH: North Atlantic Subtropical High.

During the winter half-year, the LIG NPH is weaker and less longitudinally expansive, and the AL is less deep in the Gulf of Alaska but extends further west along the Aleutian Island chain relative to the PI (Figure 5a, c, e). Correspondingly, the gradient between the AL and NPH is weaker during the LIG winter (Figure 5g), as illustrated by the large negative winter SLP pressure anomaly in the central Pacific between 20 and 50°N and the associated strong cyclonic surface wind vector anomalies (Figure 5e).

603
604
605
606
607
608
609
610
611
612
613
614
615
616
617
618
619
620
621
622
623
624
625
626
627
628
629
630
631
632
633
634
635
636
637
638
639
640
641
642
643
644
645
646
647
648

In the southwestern US, where enhanced rainfall is shown in the ensemble subset and by the proxy records, the slackened LIG SLP gradient in the Pacific may have allowed for more westerly storms to penetrate the continent, driving fewer large-scale droughts and the overall wetter winter half-year conditions relative to the PI. This pressure configuration is largely inverse that which characterized western US-wide droughts over the last 500 years (Wise 2016). These dry intervals are characterized by a strong AL, anomalously low pressure over eastern North America, and an intense high-pressure ridge centered over the Pacific Northwest, which would block storms from penetrating into the Western US and enable prolonged dry conditions. The model simulations indicate that these pressure conditions may have been less pervasive on average during the LIG winters, which could explain the enhanced southwestern US wetness simulated by the models and shown by proxy records.

The ensemble subset winter half-year moisture signal is less clear in northwestern NA, with low magnitude wet anomalies in eastern Alaska and low magnitude dry anomalies in British Columbia (Figure 4d). The weaker and westerly expanded AL and northerly wind vector anomalies in the eastern Gulf of Alaska during the LIG (Figure 5e) are characteristic of a neutral-to-strong negative Pacific Decadal Oscillation/positive North Pacific Index (-PDO/+NPI) phase (Anderson et al., 2016). However, the relationship between the strength of the AL and high latitude hydroclimate is complicated and the longitudinal position of the AL center during - PDO/+NPI states can be highly variable (Rodionov et al., 2007; Anderson et al., 2016). So, while we do observe a difference in the AL geometry between the LIG and PI that has implications for PDO/NPI dominance, given the small magnitude of the LIG winter rainfall anomalies in Alaska and western Canada, the importance of the strength and position of the AL for LIG high latitude hydroclimate is somewhat ambiguous.

During the winter half-year, the ensemble subset LIG SLP anomalies in the Gulf of Mexico and Atlantic Ocean are lower magnitude than those of the Pacific Ocean. We observe slightly higher LIG subtropical Atlantic SLPs and lower LIG SLPs in the northern Atlantic (Figure 5e) driving a moderate strengthening of the LIG latitudinal SLP gradient (Figure 5g). This configuration may indicate a slight preference for a more positive North Atlantic Oscillation (+NAO), which is associated with a steepening of the longitudinal Atlantic SLP gradient (Hurrell, 1995) and an enhancement of westerly flow (Rogers, 1990), during the LIG. A slight negative correlation exists between NAO and total winter precipitation in New England (e.g., Ning and Bradley, 2015) and other parts of the northeastern US (e.g. Morin et al., 2008), where the ensemble subset produces dry winter half-year rainfall anomalies during the LIG. The dry LIG anomalies extend throughout most of Canada in the ensemble subset winter half-year, but the correlation between NAO and modern total winter precipitation is less clear in eastern Canada (Bonsal and Shabbar, 2008; Chartrand and Pausata, 2020).

In the southeast US, the ensemble subset displays moderate northeasterly wind vector anomalies during the LIG winter half-year in the Gulf of Mexico and extending into Florida (Figure 5e). This may contribute to the wet anomalies across the southeast US during the winter half-year observed in the subset ensemble (Figure 4d), and is consistent with observations of increased fall rainfall in the region during the 20th-century (Bishop et al. 2018).

During the LIG summer half-year the model simulations produce a stronger and more expansive NPH and lower SLPs across Alaska, Canada, and most of the contiguous US relative to the PI (Figure 5b, d, f). This results in a steeper LIG latitudinal pressure gradient (Figure 5h) and strong anticyclonic surface wind vector anomalies in the north Pacific relative to the PI (Figure 5f), which may have facilitated greater delivery of oceanic moisture to the Alaska interior and western Canada, where the ensemble subset indicates enhanced wetness (Figure 4c). The wet LIG anomalies do not extend past the west coast of the US, which may be related to the westward expansion of the NPH and the corresponding enhancement of southward meridional wind vector anomalies in the east Pacific that do not penetrate the continental interior.

The Atlantic Ocean is characterized by negative pressure anomalies in the subtropics and high latitudes ($>50^{\circ}\text{N}$) during the LIG summer half-year relative to the PI (Figure 5f) and a LIG SLP gradient that is shifted northward and lower in magnitude than that of the PI (Figure 5h). The subtropical negative anomalies indicate a weakening of the NASH during the LIG, especially in the eastern Atlantic where the anomalies are largest (Figure 5f). A weakened and northward shifted NASH is associated with the warm phase of the Atlantic Meridional Oscillation (+AMO), which has been shown to drive decreased modern rainfall across the central US via diminished advection of moist, maritime air into the continental interior (Hu et al., 2011). A preference for a +AMO phase during the LIG is consistent with the dry summer half-year anomalies in the central US in the ensemble subset (Figure 4c). The warm phase of the AMO is also associated with enhanced easterly and northeasterly flow onshore flow to the southeastern US and increased summertime rainfall (Hu et al., 2011), which is reflected in the ensemble subset summer half-year easterly wind vector anomalies (Figure 5f) and positive rainfall anomalies (Figure 4c). Florida is the exception in that it is drier in the LIG ensemble subset. This may be related to the displacement of the tropical easterlies that flow south of the NASH, which leads to diminished advection of moist, unstable air to Florida and drier conditions (Coleman, 1988, Labosier and Quiring, 2013). This matches the pattern of summer half-year aridity in Florida and the Gulf of Mexico in the ensemble subset (Figure 4c) and the splitting of easterly wind vector anomalies to the north and south around Florida (Figure 5f).

Importantly, local thermodynamic forcing may also contribute to greater LIG rainfall through intensification of the hydrologic cycle (Huntington et al., 2018), especially in the northern latitudes where the enhanced seasonality of the LIG drove the largest degree of summer warming. While the clearest influence of warming on the hydrologic cycle is likely increased evaporative demand (Dai et al., 2018), it may also drive an intensification of major oceanic moisture sources for continental precipitation, especially for North America (Gimeno et al., 2013), and contribute to the observed and simulated LIG precipitation patterns.

5 Conclusions: The Last Interglacial as an analog for future moisture patterns

We present comparisons between updated MH and LIG moisture-sensitive proxy networks and model output from the latest generation of PMIP simulations to assess agreement between the two during the two most recent intervals when NH temperatures were warmer than the PI.

We find low overall agreement between our new and expanded MH proxy network and PMIP4 MH simulations, with most models producing the opposite sign and/or smaller magnitude

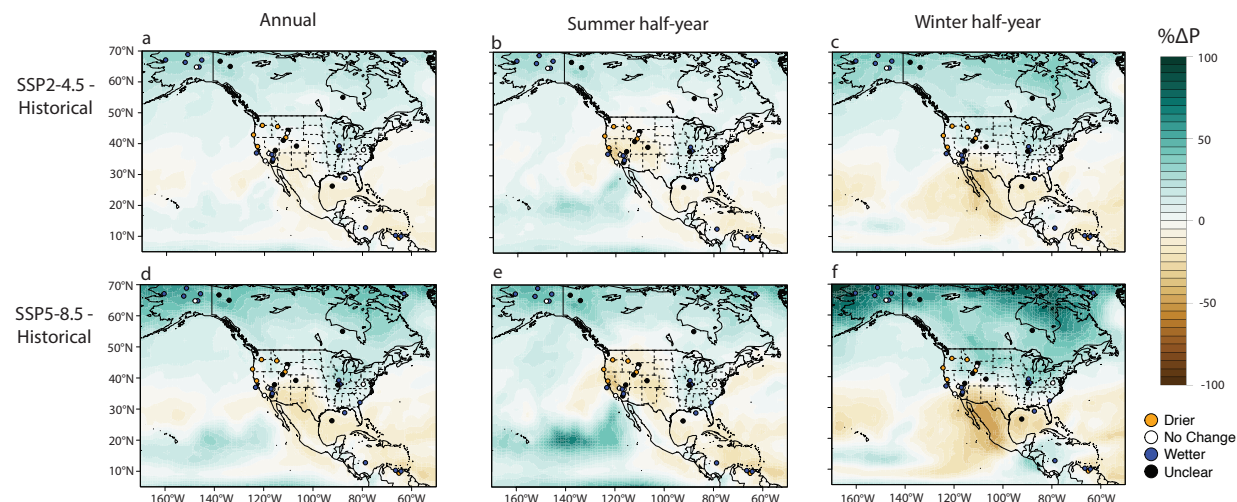
695 MH precipitation anomalies than demonstrated by the proxy network. These findings are
 696 consistent with previous comparisons between PMIP simulations and North American moisture-
 697 sensitive proxy records (Braconnot et al. 2012; Harrison et al. 2015, 2016; Hermann et al. 2018)
 698 and point toward the presence of unconstrained biases or non-linearities in the proxy records
 699 and/or the importance of climate feedbacks that are not fully represented in model simulations
 700 for NA hydroclimate during the MH.

701
 702 Agreement between our LIG proxy network and PMIP4 simulations is higher than for the
 703 MH and we find that an ensemble subset of the three models that agree most closely with the
 704 proxy network generates the highest AC2 value overall. The ensemble subset helps reconcile
 705 differences between the simulated precipitation anomalies of the full PMIP4 ensemble and the
 706 LIG proxy network in the Pacific Northwest, Rocky Mountains, northern Mississippi River
 707 Basin, and coastal southeastern US. We then use this ensemble subset to assess the seasonal
 708 patterns of LIG precipitation, with a key finding being that the NAM may have been
 709 strengthened, but not significantly expanded northward during the LIG, and that the wet
 710 anomalies of southern California LIG proxy records were primarily driven by increased
 711 southwesterly wintertime rainfall, as opposed to summertime monsoonal rainfall.
 712

713 We find that shifts in the semi-permanent pressure systems in the Atlantic and Pacific
 714 during the LIG may have impacted the amount and seasonal distribution of precipitation in much
 715 of North America. Specifically, we observe a weakening of the winter half-year LIG latitudinal
 716 SLP gradient in the Pacific and a strengthening and northward displacement of the summer half-
 717 year LIG Pacific and Atlantic SLP gradients, with important implications for moisture transport
 718 and the seasonal and spatial distribution of simulated LIG precipitation anomalies across North
 719 America.
 720

Ensemble subset

(NESM3, INM-CM4-8, CNRM-CM6)



721
 722 **Figure 6.** Annual, summer (MJJASO) and winter half-year (NDJFMA) precipitation anomalies (% change, 2071-
 723 2100 versus 1850-1949) for the SSP2-4.5 (a-c) and SSP5-8.5 (d-f) simulations in the ensemble subset. LIG proxy
 724 sites are plotted based on moisture designation for comparison with projected rainfall patterns.
 725

Comparisons between climate model simulations and proxy data from forcing scenarios that are outside the bounds of the preindustrial or historical period are critical for the evaluation of the newest generation of models (Tierney et al. 2020). However, the utility of using large ensembles of past and future climate model simulations can be limited at times because a lack of robust agreement between different models produces inconclusive results across key regions (e.g., Scussolini et al. 2019; Cook et al. 2020). Our approach may aid in navigating around this problem by providing a rationale to consider a particular subset of models based on the degree of agreement with proxy records for past time periods. Given that the LIG has been proposed as an analog for low end later 21st century radiative forcing scenarios (Burke et al., 2018), the subset of models that agree most closely with the LIG proxy network may provide more informative projections of near-future precipitation patterns relative to the full ensemble. To conclude, we evaluate our subset from the framework of both comparison with the LIG proxies and for relevancy for future hydroclimate projections.

We present precipitation anomalies between the ‘historical’ (1850-2014) simulations and two SSP (2015-2100) scenarios – SSP2-4.5 (+4.5 W m⁻²; medium forcing pathway) and SSP5-8.5 (+8.5 W m⁻²; high-end forcing pathway) for our ensemble subset that maximizes agreement with the LIG proxy record (Figure 6). On an annual basis the ensemble subset predicts increased precipitation across Alaska, Canada, the Pacific Northwest, the Great Lakes region, and the eastern US and decreased precipitation in Mexico, Texas, and the southwestern US for the SSP2-4.5 scenario (Figure 6a-c). Greater magnitude changes in the same spatial pattern are projected for the SSP5-8.5 scenario in the subset ensemble (Figure 6d-f). These findings are largely consistent with those from the model ensemble (n=13) produced by Cook et al. (2020) who observe robust wetting in Alaska, Canada, and the eastern US and drying in western and southern Mexico and Central America, but non-robust changes in the central and western US.

During the summer half-year, our ensemble subset predicts relatively more arid conditions across the already water-sensitive western US in the SSP2-4.5 simulations (Figure 6b). During the winter half-year arid conditions in the ensemble subset are projected in Mexico and extending northward into Texas, Arizona, New Mexico, and southern California (Figure 6c). The magnitude of these patterns is even greater for the SSP5-8.5 simulation (Figure 6e, f). Outside of these regions the ensemble subset shows mostly positive North American rainfall anomalies, especially in the higher latitudes (Figure 6b, c, e, f).

Qualitative comparisons between our LIG proxy network and the subset ensembles yield mixed results. Annual moisture patterns in the subset ensemble align with LIG proxy signals in some regions for the SSP2-4.5 and SSP5-8.5 simulations, like Alaska and the Midwest US where there are persistent wet anomalies on both the annual and seasonal scale relative to the historical (Figure 6). However, in other regions the alignment between the LIG proxy signals and moisture pattern predicted by the SSP simulations are more ambiguous. This includes the concentration of wet and no change proxy records in southern California and the dry proxy sites in the Pacific Northwest, where the SSP5-8.5 ensemble subsets point to enhanced aridity across both seasonal half-years (Figure 6d, e, f). The SSP2-4.5 ensemble subset is more equivocal, which is expected given the smaller overall anthropogenic forcing, but still tends drier in this region (Figure 6a, b, c). The projected annual wetness of the Pacific Northwest and Northern Rockies for the future scenarios does not align with the aridity indicated by the LIG proxies in these regions (Figure 6a,

772 d), though this comparison is complicated by the fact that summer half-years are projected to be
 773 drier under both the SSP2-4.5 and SSP5-8.5 scenarios (Figure 6b, e). This points to the difficulty
 774 of carrying out comparisons on a seasonal basis without a robust understanding of seasonal
 775 biases in the proxy records.

776
 777 Ultimately, the differences between the orbitally controlled radiative forcing of the LIG
 778 and the enhanced greenhouse effect of the end 21st century could mean that alignment between
 779 the moisture patterns of the LIG and SSP simulations is coincidental. It may be the case that
 780 other climate states from deeper time, like the Pliocene or Eocene, provide closer analogs for
 781 near future warming (Burke et al., 2018). Even so, our quantitative comparisons between an
 782 updated and expanded LIG proxy network and the newest generation of PMIP simulations can
 783 aid in the evaluation of the Earth system models that we rely on for projecting future climate
 784 states that are beyond the range of the preindustrial or historical records that models are often
 785 tuned to (Tierney et al., 2020).

786
 787 **6 Acknowledgements**
 788

789 This work was supported by NSF grants AGS-1203701, AGS-1554998, and AGS-
 790 [2102884](#) to J.L.O; and AGS-2102901 to D.E.I. We thank the modeling groups for archiving
 791 results through the CMIP5 Data Portal (<https://esgf-node.llnl.gov/search/cmip6/>). All data used
 792 in model-proxy comparisons are available in the supporting information and are available for
 793 download from the NOAA National Climatic Data Center's Paleoclimatology database. R scripts
 794 used to process and analyze climate model data and carry out comparisons with proxy networks
 795 are available upon from the authors.

796
 797 **References**

- 798 Adam, D. P., and West, G. J. (1983). Temperature and Precipitation Estimates Through the Last
 799 Glacial Cycle from Clear Lake, California, Pollen Data. *Science*, 219(4581), 168 LP – 170.
 800 <https://doi.org/10.1126/science.219.4581.168>
- 801 Anderson, L., Berkelhammer, M., Barron, J. A., Steinman, B. A., Finney, B. P., & Abbott, M. B.
 802 (2016). Lake oxygen isotopes as recorders of North American Rocky Mountain
 803 hydroclimate: Holocene patterns and variability at multi-decadal to millennial time scales.
 804 *Global and Planetary Change*, 137, 131–148.
 805 <https://doi.org/https://doi.org/10.1016/j.gloplacha.2015.12.021>
- 806 Anderson, R. S., Jiménez-Moreno, G., Ager, T., & Porinchu, D. F. (2014). High-elevation
 807 paleoenvironmental change during MIS 6–4 in the central Rockies of Colorado as
 808 determined from pollen analysis. *Quaternary Research*, 82(3), 542–552.
 809 <https://doi.org/DOI: 10.1016/j.yqres.2014.03.005>
- 810 Baker, R. G. (1986). Sangamonian(?) and Wisconsinan paleoenvironments in Yellowstone
 811 National Park. *GSA Bulletin*, 97(6), 717–736. [https://doi.org/10.1130/0016-7606\(1986\)97<717:SAWPIY>2.0.CO;2](https://doi.org/10.1130/0016-7606(1986)97<717:SAWPIY>2.0.CO;2)
- 812 Balch, D. P., Cohen, A. S., Schnurrenberger, D. W., Haskell, B. J., Valero Garces, B. L., Beck, J.
 813 W., Cheng, H., & Edwards, R. L. (2005). Ecosystem and paleohydrological response to
 814 Quaternary climate change in the Bonneville Basin, Utah. *Palaeogeography,*
 815

- 816 *Palaeoclimatology, Palaeoecology*, 221(1), 99–122.
 817 <https://doi.org/https://doi.org/10.1016/j.palaeo.2005.01.013>
- 818 Baldini, L. M., Baldini, J. U. L., McElwaine, J. N., Frappier, A. B., Asmerom, Y., Liu, K.,
 819 Prufer, K. M., Ridley, H. E., Polyak, V., Kennett, D. J., Macpherson, C. G., Aquino, V. V.,
 820 Awe, J., & Breitenbach, S. F. M. (2016). Persistent northward North Atlantic tropical
 821 cyclone track migration over the past five centuries. *Scientific Reports*, 6(1), 37522.
 822 <https://doi.org/10.1038/srep37522>
- 823 Bartlein, P. J., Anderson, K. H., Anderson, P. M., Edwards, M. E., Mock, C. J., Thompson, R. S.,
 824 Webb, R. S., Webb III, T., & Whitlock, C. (1998). Paleoclimate simulations for North
 825 America over the past 21,000 years: features of the simulated climate and comparisons with
 826 paleoenvironmental data. *Quaternary Science Reviews*, 17(6), 549–585.
 827 [https://doi.org/https://doi.org/10.1016/S0277-3791\(98\)00012-2](https://doi.org/https://doi.org/10.1016/S0277-3791(98)00012-2)
- 828 Bartlein, P. J., Harrison, S. P., & Izumi, K. (2017). Underlying causes of Eurasian
 829 midcontinental aridity in simulations of mid-Holocene climate. *Geophysical Research
 830 Letters*, 44(17), 9020–9028. <https://doi.org/https://doi.org/10.1002/2017GL074476>
- 831 Bigelow, N. H., Edwards, M. E., Elias, S. A., Hamilton, T. D., & Schweger, C. E. (2014).
 832 Tundra and boreal forest of interior Alaska during terminal MIS 6 and MIS 5e. *Vegetation
 833 History and Archaeobotany*, 23(3), 177–193. <https://doi.org/10.1007/s00334-013-0425-z>
- 834 Bishop, D. A., Williams, A. P., Seager, R., Fiore, A. M., Cook, B. I., Mankin, J. S., Singh, D.,
 835 Smerdon, J. E., & Rao, M. P. (2018). Investigating the causes of increased 20(th)-century
 836 fall precipitation over the southeastern United States. *Journal of Climate*, 32(2), 575–590.
 837 <https://doi.org/10.1175/JCLI-D-18-0244.1>
- 838 Bonsal, B., & Shabbar, A. (2008). Impacts of Large-Scale Circulation Variability on Low
 839 Streamflows over Canada: A Review. *Canadian Water Resources Journal / Revue
 840 Canadienne Des Ressources Hydriques*, 33(2), 137–154.
 841 <https://doi.org/10.4296/cwrj3302137>
- 842 Braconnot, P., Harrison, S. P., Kageyama, M., Bartlein, P. J., Masson-Delmotte, V., Abe-Ouchi, A., Otto-Bliesner, B., & Zhao, Y. (2012). Evaluation of climate models using palaeoclimatic data. *Nature Climate Change*, 2(6), 417–424.
 843 <https://doi.org/10.1038/nclimate1456>
- 844 Brewer, S., Guiot, J., Sánchez-Goñi, M. F., & Klotz, S. (2008). The climate in Europe during the
 845 Eemian: a multi-method approach using pollen data. *Quaternary Science Reviews*, 27(25),
 846 2303–2315. <https://doi.org/https://doi.org/10.1016/j.quascirev.2008.08.029>
- 847 Brierley, C. M., Zhao, A., Harrison, S. P., Braconnot, P., Williams, C. J. R., Thornalley, D. J. R.,
 848 Shi, X., Peterschmitt, J.-Y., Ohgaito, R., Kaufman, D. S., Kageyama, M., Hargreaves, J. C.,
 849 Erb, M. P., Emile-Geay, J., D'Agostino, R., Chandan, D., Carré, M., Bartlein, P. J., Zheng,
 850 W., ... Abe-Ouchi, A. (2020). Large-scale features and evaluation of the PMIP4-CMIP6
 851 \textit{midHolocene} simulations. *Climate of the Past*, 16(5), 1847–1872.
 852 <https://doi.org/10.5194/cp-16-1847-2020>
- 853 Burke, K. D., Williams, J. W., Chandler, M., Haywood, A., Lunt, D., & Otto-Bliesner, B. (2018).
 854 Pliocene and Eocene provide best analogs for near-future climates. *Proceedings of the
 855 National Academy of Sciences*, 115, 13288–13293.
- 856 Cárdenes-Sandí, G. M., Shadik, C. R., Correa-Metrio, A., Gosling, W. D., Cheddadi, R., & Bush,
 857 M. B. (2019). Central American climate and microrefugia: A view from the last interglacial.
 858 *Quaternary Science Reviews*, 205, 224–233.
 859 <https://doi.org/https://doi.org/10.1016/j.quascirev.2018.12.021>

- 862 Chartrand, J., & Pausata, F. S. R. (2020). Impacts of the North Atlantic Oscillation on winter
863 precipitations and storm track variability in southeast Canada and the northeast United
864 States. *Weather and Climate Dynamics*, 1(2), 731–744. <https://doi.org/10.5194/wcd-1-731-2020>
- 865 Chartrand, J., & Pausata, F. S. R. (2020). Impacts of the North Atlantic Oscillation on winter
866 precipitations and storm track variability in southeast Canada and the northeast United
867 States. *Weather and Climate Dynamics*, 1(2), 731–744. <https://doi.org/10.5194/wcd-1-731-2020>
- 868 Coleman, J. (1988). Climatic warming and increased summer aridity in Florida, U.S.A. *Climatic
869 Change*, 12, 165–178. <https://doi.org/10.1007/BF00138937>
- 870 Conroy, J. L., Karamperidou, C., Grimley, D. A., & Guenthner, W. R. (2019). Surface winds
871 across eastern and midcontinental North America during the Last Glacial Maximum: A new
872 data-model assessment. *Quaternary Science Reviews*, 220(August), 14–29.
873 <https://doi.org/10.1016/j.quascirev.2019.07.003>
- 874 Consortium, P. H. (2017). Comparing proxy and model estimates of hydroclimate variability and
875 change over the Common Era. *Clim. Past*, 13(12), 1851–1900. <https://doi.org/10.5194/cp-13-1851-2017>
- 876 Cook, B. I., Mankin, J. S., Marvel, K., Williams, A. P., Smerdon, J. E., & Anchukaitis, K. J.
877 (2020). Twenty-First Century Drought Projections in the CMIP6 Forcing Scenarios. *Earth's
878 Future*, 8(6), e2019EF001461. <https://doi.org/10.1029/2019EF001461>
- 879 Curry, B. B., & Baker, R. G. (2000). Palaeohydrology, vegetation, and climate since the late
880 Illinois Episode (~130 ka) in south-central Illinois. *Palaeogeography, Palaeoclimatology,
881 Palaeoecology*, 155(1), 59–81. [https://doi.org/10.1016/S0031-0182\(99\)00094-2](https://doi.org/10.1016/S0031-0182(99)00094-2)
- 882 D., B. K., W., W. J., A., C. M., M., H. A., J., L. D., & L., O.-B. B. (2018). Pliocene and Eocene
883 provide best analogs for near-future climates. *Proceedings of the National Academy of
884 Sciences*, 115(52), 13288–13293. <https://doi.org/10.1073/pnas.1809600115>
- 885 Dai, A., Zhao, T., & Chen, J. (2018). Climate Change and Drought: a Precipitation and
886 Evaporation Perspective. *Current Climate Change Reports*, 4(3), 301–312.
887 <https://doi.org/10.1007/s40641-018-0101-6>
- 888 Dalmonech, D., Zaehle, S., Schürmann, G., Brovkin, V., Reick, C., & Schnur, R. (2015).
889 Separation of the Effects of Land and Climate Model Errors on Simulated Contemporary
890 Land Carbon Cycle Trends in the MPI Earth System Model version 1*. *Journal of Climate*,
891 28, 272–291. <https://doi.org/10.1175/JCLI-D-13-00593.1>
- 892 Delire, C., Levis, S., Bonan, G., Foley, J., Coe, M., & Vavrus, S. (2002). Comparison of the
893 climate simulated by the CCM3 coupled to two different land-surface models. *Climate
894 Dynamics*, 19(8), 657–669. <https://doi.org/10.1007/s00382-002-0255-7>
- 895 Deposits, P. N., Hudson, I., Lowland, B., & Wyatt, P. H. (1990). Amino Acid Evidence
896 Indicating Two or More Ages of Pre-Holocene Nonglacial Deposits In Hudson Bay
897 Lowland, Northern Ontario. *Géographie Physique et Quaternaire*.
- 898 Diem, J. E. (2013). Influences of the Bermuda High and atmospheric moistening on changes in
899 summer rainfall in the Atlanta, Georgia region, USA. *International Journal of Climatology*,
900 33(1), 160–172. <https://doi.org/10.1002/joc.3421>
- 901 Diffenbaugh, N. S., Swain, D. L., & Touma, D. (2015). Anthropogenic warming has increased
902 drought risk in California. *Proceedings of the National Academy of Sciences*, 112(13),
903 3931–3936. <https://doi.org/10.1073/pnas.1422385112>

- 908 Feng, R., Bhattacharya, T., Otto-Bliesner, B. L., Brady, E. C., Haywood, A. M., Tindall, J. C.,
909 Hunter, S. J., Abe-Ouchi, A., Chan, W. Le, Kageyama, M., Contoux, C., Guo, C., Li, X.,
910 Lohmann, G., Stepanek, C., Tan, N., Zhang, Q., Zhang, Z., Han, Z., ... Peltier, W. R.
911 (2022). Past terrestrial hydroclimate sensitivity controlled by Earth system feedbacks.
912 *Nature Communications*, 13(1), 1–11. <https://doi.org/10.1038/s41467-022-28814-7>
- 913 Fischer, H., Meissner, K. J., Mix, A. C., Abram, N. J., Austermann, J., Brovkin, V., Capron, E.,
914 Colombaroli, D., Daniau, A. L., Dyez, K. A., Felis, T., Finkelstein, S. A., Jaccard, S. L.,
915 McClymont, E. L., Rovere, A., Sutter, J., Wolff, E. W., Affolter, S., Bakker, P., ... Zhou, L.
916 (2018). Palaeoclimate constraints on the impact of 2 °C anthropogenic warming and beyond.
917 *Nature Geoscience*, 11(7), 474–485. <https://doi.org/10.1038/s41561-018-0146-0>
- 918 Forester, R. M., Lowenstein, T. K., & Spencer, R. J. (2005). An ostracode based paleolimnologic
919 and paleohydrologic history of Death Valley: 200 to 0 ka. *GSA Bulletin*, 117(11–12), 1379–
920 1386. <https://doi.org/10.1130/B25637.1>
- 921 Gavin, D., & Brubaker, L. (2015). *Late Pleistocene and Holocene Environmental Change on the
922 Olympic Peninsula, Washington*. 222. <https://doi.org/10.1007/978-3-319-11014-1>
- 923 Gimeno, L., Nieto, R., Drumond, A., Castillo, R., & Trigo, R. (2013). Influence of the
924 intensification of the major oceanic moisture sources on continental precipitation.
925 *Geophysical Research Letters*, 40(7), 1443–1450.
926 <https://doi.org/https://doi.org/10.1002/grl.50338>
- 927 Glover, K. C., MacDonald, G. M., Kirby, M. E., Rhodes, E. J., Stevens, L., Silveira, E.,
928 Whitaker, A., & Lydon, S. (2017). Evidence for orbital and North Atlantic climate forcing
929 in alpine Southern California between 125 and 10 ka from multi-proxy analyses of Baldwin
930 Lake. *Quaternary Science Reviews*, 167, 47–62.
931 <https://doi.org/https://doi.org/10.1016/j.quascirev.2017.04.028>
- 932 Grayson, D. K. (2000). Mammalian responses to Middle Holocene climatic change in the Great
933 Basin of the western United States. *Journal of Biogeography*, 27(1), 181–192.
934 <https://doi.org/https://doi.org/10.1046/j.1365-2699.2000.00383.x>
- 935 Greve, P., Orlowsky, B., Mueller, B., Sheffield, J., Reichstein, M., & Seneviratne, S. I. (2014).
936 Global assessment of trends in wetting and drying over land. *Nature Geoscience*, 7(10),
937 716–721. <https://doi.org/10.1038/ngeo2247>
- 938 Gwet, K. (2015). Testing the Difference of Correlated Agreement Coefficients for Statistical
939 Significance. *Educational and Psychological Measurement*, 76.
940 <https://doi.org/10.1177/0013164415596420>
- 941 Gwet, K. L. (2008). Computing inter-rater reliability and its variance in the presence of high
942 agreement. *British Journal of Mathematical and Statistical Psychology*, 61(1), 29–48.
943 <https://doi.org/10.1348/000711006X126600>
- 944 Hardt, B., Rowe, H. D., Springer, G. S., Cheng, H., & Edwards, R. L. (2010). The seasonality of
945 east central North American precipitation based on three coeval Holocene speleothems from
946 southern West Virginia. *Earth and Planetary Science Letters*, 295(3), 342–348.
947 <https://doi.org/https://doi.org/10.1016/j.epsl.2010.04.002>
- 948 Harrison, S. P., Kutzbach, J.-E., Liu, Z., Bartlein, P. J., Otto-Bliesner, B., Muhs, D., Prentice, I.
949 C., & Thompson, R. S. (2003). Mid-Holocene climates of the Americas: a dynamical
950 response to changed seasonality. *Climate Dynamics*, 20(7–8), 663–688.
951 <https://doi.org/10.1007/s00382-002-0300-6>

- 952 Hermann, N. W., Oster, J. L., & Ibarra, D. E. (2018). Spatial patterns and driving mechanisms of
953 mid-Holocene hydroclimate in western North America. *Journal of Quaternary Science*,
954 33(4), 421–434. <https://doi.org/10.1002/jqs.3023>
- 955 Heusser, L. E. (2000). Rapid oscillations in western North America vegetation and climate
956 during oxygen isotope stage 5 inferred from pollen data from Santa Barbara Basin (Hole
957 893A). *Palaeogeography, Palaeoclimatology, Palaeoecology*, 161(3), 407–421.
958 [https://doi.org/https://doi.org/10.1016/S0031-0182\(00\)00096-1](https://doi.org/https://doi.org/10.1016/S0031-0182(00)00096-1)
- 959 Hu, Q., Feng, S., & Oglesby, R. J. (2011). Variations in North American Summer Precipitation
960 Driven by the Atlantic Multidecadal Oscillation. *Journal of Climate*, 24(21), 5555–5570.
961 <https://doi.org/10.1175/2011JCLI4060.1>
- 962 Huntington, T. G., Weiskel, P. K., Wolock, D. M., & McCabe, G. J. (2018). A new indicator
963 framework for quantifying the intensity of the terrestrial water cycle. *Journal of Hydrology*,
964 559, 361–372. <https://doi.org/https://doi.org/10.1016/j.jhydrol.2018.02.048>
- 965 Hurrell, J. W. (1995). Decadal Trends in the North Atlantic Oscillation. *Science (New York,*
966 *N.Y.*), 269, 676–679. <https://doi.org/10.1126/science.269.5224.676>
- 967 Ibarra, D. E., Oster, J. L., Winnick, M. J., Caves Rugenstein, J. K., Byrne, M. P., & Chamberlain,
968 C. P. (2018). Warm and cold wet states in the western United States during the Pliocene–
969 Pleistocene. *Geology*, 46(4), 355–358. <https://doi.org/10.1130/G39962.1>
- 970 Jiménez-Moreno, G., Scott Anderson, R., & Fawcett, P. J. (2007). Orbital- and millennial-scale
971 vegetation and climate changes of the past 225ka from Bear Lake, Utah–Idaho (USA).
972 *Quaternary Science Reviews*, 26(13), 1713–1724.
973 <https://doi.org/https://doi.org/10.1016/j.quascirev.2007.05.001>
- 974 Kaufman, D., McKay, N., Routson, C., Erb, M., Dätwyler, C., Sommer, P. S., Heiri, O., &
975 Davis, B. (2020). Holocene global mean surface temperature, a multi-method reconstruction
976 approach. *Scientific Data*, 7(1), 201. <https://doi.org/10.1038/s41597-020-0530-7>
- 977 Knight, C., Dorale, J., & Edwards, R. (2006). Stalagmite Records of Interglacial and Glacial
978 Flooding at Crevice Cave, Missouri, USA. *AGU Fall Meeting Abstracts*.
- 979 Kwiecien, O., Braun, T., Brunello, C. F., Faulkner, P., Hausmann, N., Helle, G., Hoggarth, J. A.,
980 Ionita, M., Jazwa, C. S., Kelmelis, S., Marwan, N., Nava-Fernandez, C., Nehme, C., Opel,
981 T., Oster, J. L., Perșoiu, A., Petrie, C., Pruffer, K., Saarni, S. M., ... Breitenbach, S. F. M.
982 (2022). What we talk about when we talk about seasonality – A transdisciplinary review.
983 *Earth-Science Reviews*, 225, 103843.
984 <https://doi.org/https://doi.org/10.1016/j.earscirev.2021.103843>
- 985 Labosier, C. F., & Quiring, S. M. (2013). Hydroclimatology of the southeastern USA. *Climate*
986 *Research*, 57(2), 157–171. <https://doi.org/10.3354/cr01166>
- 987 Lapointe, F., Francus, P., Lamoureux, S. F., Vuille, M., Jenny, J. P., Bradley, R. S., & Massa, C.
988 (2017). Influence of North Pacific decadal variability on the western Canadian Arctic over
989 the past 700 years. *Climate of the Past*, 13(4), 411–420. <https://doi.org/10.5194/cp-13-411-2017>
- 990 Li, W., Li, L., Fu, R., Deng, Y., & Wang, H. (2011). Changes to the North Atlantic Subtropical
991 High and Its Role in the Intensification of Summer Rainfall Variability in the Southeastern
992 United States. *Journal of Climate*, 24(5), 1499–1506.
993 <https://doi.org/10.1175/2010JCLI3829.1>
- 994 LIGA members, Anderson, P., Borisova, O., de Beaulieu, J.-L., de Vernal, A., Eiriksson, J.,
995 Funder, S., Gibbard, P., Hamilton, T., Harrison, S. P., Houmark-Nielsen, M., Huntley, B.,
996 Knudsen, K. L., Larsen, E., Maher, L. J., Matthews, J. V., Miller, G., Raukas, A., Reeh, N.,

- 998 ... Ward, B. (1991). Report of 1st discussion group: The last interglacial in high latitudes of
 999 the Northern Hemisphere: Terrestrial and marine evidence. *Quaternary International*, 10–
 1000 12, 9–28. [https://doi.org/https://doi.org/10.1016/1040-6182\(91\)90038-P](https://doi.org/10.1016/1040-6182(91)90038-P)
- 1001 Limoges, A., de Vernal, A., & Van Nieuwenhove, N. (2014). Long-term hydrological changes in
 1002 the northeastern Gulf of Mexico (ODP-625B) during the Holocene and late Pleistocene
 1003 inferred from organic-walled dinoflagellate cysts. *Palaeogeography, Palaeoclimatology,*
 1004 *Palaeoecology*, 414, 178–191. [https://doi.org/https://doi.org/10.1016/j.palaeo.2014.08.019](https://doi.org/10.1016/j.palaeo.2014.08.019)
- 1005 Lindstrom, S. (1990). Submerged Tree Stumps as Indicators of Mid-Holocene Aridity in the
 1006 Lake Tahoe Region. *Journal of California and Great Basin Anthropology*, 12(2), 146–157.
 1007 <http://www.jstor.org/stable/10.2307/27825419>
- 1008 Lora, J. M., & Ibarra, D. E. (2019). The North American hydrologic cycle through the last
 1009 deglaciation. *Quaternary Science Reviews*, 226, 105991.
 1010 <https://doi.org/https://doi.org/10.1016/j.quascirev.2019.105991>
- 1011 Lyle, M., Heusser, L., Ravelo, C., Andreasen, D., Olivarez Lyle, A., & Diffenbaugh, N. (2010).
 1012 Pleistocene water cycle and eastern boundary current processes along the California
 1013 continental margin. *Paleoceanography*, 25(4).
 1014 <https://doi.org/https://doi.org/10.1029/2009PA001836>
- 1015 Mantua, N. J., & Hare, S. R. (2002). The Pacific Decadal Oscillation. In *Journal of*
 1016 *Oceanography* (Vol. 58, Issue 1, pp. 35–44). <https://doi.org/10.1023/A:1015820616384>
- 1017 Marcott, S. A., Shakun, J. D., Clark, P. U., & Mix, A. C. (2013). A Reconstruction of Regional
 1018 and Global Temperature for the Past 11,300 Years. *Science*, 339(6124), 1198–1201.
 1019 <https://doi.org/10.1126/science.1228026>
- 1020 Mauri, A., Davis, B. A. S., Collins, P. M., & Kaplan, J. O. (2014). The influence of atmospheric
 1021 circulation on the mid-Holocene climate of Europe: a data–model comparison. *Climate of*
 1022 *the Past*, 10(5), 1925–1938. <https://doi.org/10.5194/cp-10-1925-2014>
- 1023 Members, C. L. I. P. (2006). Last Interglacial Arctic warmth confirms polar amplification of
 1024 climate change. *Quaternary Science Reviews*, 25(13), 1383–1400.
 1025 <https://doi.org/https://doi.org/10.1016/j.quascirev.2006.01.033>
- 1026 Miller, G. H., Alley, R. B., Brigham-Grette, J., Fitzpatrick, J. J., Polyak, L., Serreze, M. C., &
 1027 White, J. W. C. (2010). Arctic amplification: Can the past constrain the future? *Quaternary*
 1028 *Science Reviews*, 29(15–16), 1779–1790. <https://doi.org/10.1016/j.quascirev.2010.02.008>
- 1029 Miller, I. M., Pigati, J. S., Scott Anderson, R., Johnson, K. R., Mahan, S. A., Ager, T. A., Baker,
 1030 R. G., Blaauw, M., Bright, J., Brown, P. M., Bryant, B., Calamari, Z. T., Carrara, P. E.,
 1031 Cherney, M. D., Demboski, J. R., Elias, S. A., Fisher, D. C., Gray, H. J., Haskett, D. R., ...
 1032 Wilson, J. (2014). Summary of the Snowmastodon Project Special Volume: A high-
 1033 elevation, multi-proxy biotic and environmental record of MIS 6–4 from the Ziegler
 1034 Reservoir fossil site, Snowmass Village, Colorado, USA. *Quaternary Research*, 82(3), 618–
 1035 634. <https://doi.org/https://doi.org/10.1016/j.yqres.2014.07.004>
- 1036 Montero-Serrano, J.-C., Bout-Roumazeilles, V., Carlson, A. E., Tribouillard, N., Bory, A.,
 1037 Meunier, G., Sionneau, T., Flower, B. P., Martinez, P., Billy, I., & Riboulleau, A. (2011).
 1038 Contrasting rainfall patterns over North America during the Holocene and Last Interglacial
 1039 as recorded by sediments of the northern Gulf of Mexico. *Geophysical Research Letters*,
 1040 38(14). <https://doi.org/https://doi.org/10.1029/2011GL048194>
- 1041 Morin, J., Block, P., Rajagopalan, B., & Clark, M. (2008). Identification of large scale climate
 1042 patterns affecting snow variability in the eastern United States. *International Journal of*
 1043 *Climatology*, 28(3), 315–328. <https://doi.org/https://doi.org/10.1002/joc.1534>

- 1044 Muhs, D. R., Ager, T. A., & Begét, J. E. (2001). Vegetation and paleoclimate of the last
1045 interglacial period, central Alaska. *Quaternary Science Reviews*, 20(1), 41–61.
1046 [https://doi.org/https://doi.org/10.1016/S0277-3791\(00\)00132-3](https://doi.org/https://doi.org/10.1016/S0277-3791(00)00132-3)
- 1047 Ning, L., & Bradley, R. (2015). Winter Climate Extremes over the Northeastern United States
1048 and Southeastern Canada and Teleconnections with Large-Scale Modes of Climate
1049 Variability*. *Journal of Climate*, 28, 2475–2493. <https://doi.org/10.1175/JCLI-D-13-00750.1>
- 1051 Osman, M. B., Tierney, J. E., Zhu, J., Tardif, R., Hakim, G. J., King, J., & Poulsen, C. J. (2021).
1052 Globally resolved surface temperatures since the Last Glacial Maximum. *Nature*,
1053 599(7884), 239–244. <https://doi.org/10.1038/s41586-021-03984-4>
- 1054 Oster, J.L., Ibarra, D.E., 2019, Glacial hydroclimate of western North America: Insights from
1055 proxy-model comparison and implications for Lake Bonneville. *Proceedings Volume: 2018*
1056 *Lake Bonneville Geologic Conference and Short Course*, Lund, W.R., McKean, A.P.,
1057 Bowman, S.D (eds) Utah Geological Survey Miscellaneous Publication 170.
- 1058 Oster, J. L., Ibarra, D. E., Winnick, M. J., & Maher, K. (2015). Steering of westerly storms over
1059 western North America at the Last Glacial Maximum. *Nature Geoscience*, 8(3), 201–205.
1060 <https://doi.org/10.1038/ngeo2365>
- 1061 Otto-Bliesner, B. L., Brady, E. C., Zhao, A., Brierley, C. M., Axford, Y., Capron, E., Govin, A.,
1062 Hoffman, J. S., Isaacs, E., Kageyama, M., Scussolini, P., Tzedakis, P. C., Williams, C. J. R.,
1063 Wolff, E., Abe-Ouchi, A., Braconnot, P., Ramos Buarque, S., Cao, J., De Vernal, A., ...
1064 Zheng, W. (2021). Large-scale features of Last Interglacial climate: Results from evaluating
1065 the lig127k simulations for the Coupled Model Intercomparison Project (CMIP6)-
1066 Paleoclimate Modeling Intercomparison Project (PMIP4). *Climate of the Past*, 17(1), 63–
1067 94. <https://doi.org/10.5194/cp-17-63-2021>
- 1068 Otto-Bliesner, B., Braconnot, P., Harrison, S., Lunt, D., Abe-Ouchi, A., Albani, S., Bartlein, P.,
1069 Capron, E., Carlson, A., Dutton, A., Fischer, H., Goelzer, H., Govin, A., Haywood, A.,
1070 Joos, F., LeGrande, A., Lipscomb, W., Lohmann, G., Mahowald, N., & Zhang, Q. (2017).
1071 The PMIP4 contribution to CMIP6 – Part 2: Two interglacials, scientific objective and
1072 experimental design for Holocene and Last Interglacial simulations. *Geosci. Model Dev.*,
1073 10, 3979–4003. <https://doi.org/10.5194/gmd-10-3979-2017>
- 1074 Pewe, T. L., Berger, G. W., Westgate, J. A., Brown, P. M., & Leavitt, S. W. (1997). Eva
1075 interglaciation forest bed, unglaciated East-Central Alaska: Global warming 125,000 years
1076 ago. In T. L. Péwé, G. W. Berger, J. A. Westgate, P. M. Brown, & S. W. Leavitt (Eds.), *Eva*
1077 *interglaciation forest bed, unglaciated East-Central Alaska: global warming 125,000 years*
1078 *ago* (Vol. 319, p. 0). Geological Society of America. <https://doi.org/10.1130/0-8137-2319-1.1>
- 1080 Pierce, K. L., Muhs, D. R., Fosberg, M. A., Mahan, S. A., Rosenbaum, J. G., Licciardi, J. M., &
1081 Pavich, M. J. (2011). A loess–paleosol record of climate and glacial history over the past
1082 two glacial–interglacial cycles (~150ka), southern Jackson Hole, Wyoming. *Quaternary*
1083 *Research*, 76(1), 119–141. <https://doi.org/https://doi.org/10.1016/j.yqres.2011.03.006>
- 1084 Pisias, N. G., Martinson, D. G., Moore, T. C., Shackleton, N. J., Prell, W., Hays, J., & Boden, G.
1085 (1984). High resolution stratigraphic correlation of benthic oxygen isotopic records
1086 spanning the last 300,000 years. *Marine Geology*, 56(1), 119–136.
1087 [https://doi.org/https://doi.org/10.1016/0025-3227\(84\)90009-4](https://doi.org/https://doi.org/10.1016/0025-3227(84)90009-4)
- 1088 Pisias, N. G., Mix, A. C., & Heusser, L. (2001). Millennial scale climate variability of the
1089 northeast Pacific Ocean and northwest North America based on radiolaria and pollen.

- 1090 *Quaternary Science Reviews*, 20(14), 1561–1576.
 1091 [https://doi.org/https://doi.org/10.1016/S0277-3791\(01\)00018-X](https://doi.org/https://doi.org/10.1016/S0277-3791(01)00018-X)
- 1092 Reheis, M. C., Bright, J., Lund, S. P., Miller, D. M., Skipp, G., & Fleck, R. J. (2012). A half-
 1093 million-year record of paleoclimate from the Lake Manix Core, Mojave Desert, California.
 1094 *Palaeogeography, Palaeoclimatology, Palaeoecology*, 365–366, 11–37.
 1095 <https://doi.org/https://doi.org/10.1016/j.palaeo.2012.09.002>
- 1096 Riboulleau, A., Bout-Roumazeilles, V., & Tribouillard, N. (2014). Controls on detrital
 1097 sedimentation in the Cariaco Basin during the last climatic cycle: insight from clay
 1098 minerals. *Quaternary Science Reviews*, 94, 62–73.
 1099 <https://doi.org/https://doi.org/10.1016/j.quascirev.2014.04.023>
- 1100 Rodionov, S. N., Bond, N. A., & Overland, J. E. (2007). The Aleutian Low, storm tracks, and
 1101 winter climate variability in the Bering Sea. *Deep Sea Research Part II: Topical Studies in
 1102 Oceanography*, 54(23), 2560–2577.
 1103 <https://doi.org/https://doi.org/10.1016/j.dsr2.2007.08.002>
- 1104 Rogers, J. (1990). Patterns of Low-Frequency Monthly Sea Level Pressure Variability (1899–
 1105 1986) and Associated Wave Cyclone Frequencies. *Journal of Climate*, 3, 1364–1379.
 1106 [https://doi.org/10.1175/1520-0442\(1990\)003<1364:POLFMS>2.0.CO;2](https://doi.org/10.1175/1520-0442(1990)003<1364:POLFMS>2.0.CO;2)
- 1107 Scheff, J. (2018). Drought Indices, Drought Impacts, CO₂, and Warming: a Historical and
 1108 Geologic Perspective. *Current Climate Change Reports*, 4(2), 202–209.
 1109 <https://doi.org/10.1007/s40641-018-0094-1>
- 1110 Schmidt, G. A., Annan, J. D., Bartlein, P. J., Cook, B. I., Guilyardi, E., Hargreaves, J. C.,
 1111 Harrison, S. P., Kageyama, M., Legrande, A. N., Konecky, B., Lovejoy, S., Mann, M. E.,
 1112 Masson-Delmotte, V., Risi, C., Thompson, D., Timmermann, A., & Yiou, P. (2014). Using
 1113 palaeo-climate comparisons to constrain future projections in CMIP5. *Climate of the Past*,
 1114 10(1), 221–250. <https://doi.org/10.5194/cp-10-221-2014>
- 1115 Schmidt, M. W., & Spero, H. J. (2011). Meridional shifts in the marine ITCZ and the tropical
 1116 hydrologic cycle over the last three glacial cycles. *Paleoceanography*, 26(1).
 1117 <https://doi.org/https://doi.org/10.1029/2010PA001976>
- 1118 Schneider, U., Becker, A., Finger, P., Meyer-Christoffer, A., Rudolf, B., Ziese, M., 2011. GPCC
 1119 full data reanalysis version 6.0 at 0.5°: Monthly landsurface precipitation from rain-gauges
 1120 built on gts-based and historic data.
- 1121 Schweger, C. E., & Matthews, J. V. (1991). The last (Koy-Yukon) interglaciation in the Yukon:
 1122 Comparisons with holocene and interstadial pollen records. *Quaternary International*, 10–
 1123 12, 85–94. [https://doi.org/https://doi.org/10.1016/1040-6182\(91\)90042-M](https://doi.org/https://doi.org/10.1016/1040-6182(91)90042-M)
- 1124 Sharpe, S. E., & Bright, J. (2014). A high-elevation MIS 5 hydrologic record using mollusks and
 1125 ostracodes from Snowmass Village, Colorado, USA. *Quaternary Research*, 82(3), 604–617.
 1126 <https://doi.org/https://doi.org/10.1016/j.yqres.2014.01.014>
- 1127 Springer, G. S., Rowe, H. D., Hardt, B., Cheng, H., & Edwards, R. L. (2014). East central North
 1128 America climates during marine isotope stages 3–5. *Geophysical Research Letters*, 41(9),
 1129 3233–3237. <https://doi.org/https://doi.org/10.1002/2014GL059884>
- 1130 Suh, Y. J., Diefendorf, A. F., Freimuth, E. J., & Hyun, S. (2020). Last interglacial (MIS 5e) and
 1131 Holocene paleohydrology and paleovegetation of midcontinental North America from Gulf
 1132 of Mexico sediments. *Quaternary Science Reviews*, 227, 106066.
 1133 <https://doi.org/https://doi.org/10.1016/j.quascirev.2019.106066>
- 1134 Sundqvist, H. S., Kaufman, D. S., McKay, N. P., Balascio, N. L., Briner, J. P., Cwynar, L. C.,
 1135 Sejrup, H. P., Seppä, H., Subetto, D. A., Andrews, J. T., Axford, Y., Bakke, J., Birks, H. J.

- 1136 B., Brooks, S. J., de Vernal, A., Jennings, A. E., Ljungqvist, F. C., Rühland, K. M., Saenger,
1137 C., ... Viau, A. E. (2014). Arctic Holocene proxy climate database – new approaches
1138 to assessing geochronological accuracy and encoding climate variables. *Climate of the Past*,
1139 10(4), 1605–1631. <https://doi.org/10.5194/cp-10-1605-2014>
- 1140 Swain, D. L., Tsiang, M., Haugen, M., Singh, D., Charland, A., Rajaratnam, B., & Diffenbaugh,
1141 N. S. (2014). THE EXTRAORDINARY CALIFORNIA DROUGHT OF 2013/2014:
1142 CHARACTER, CONTEXT, AND THE ROLE OF CLIMATE CHANGE. *Bulletin of the*
1143 *American Meteorological Society*, 95(9), S3–S7.
1144 <http://proxy.library.vanderbilt.edu/login?url=https://www.proquest.com/scholarly-journals/extraordinary-california-drought-2013-2014/docview/1623231385/se-2?accountid=14816>
- 1145 Swann, A. L. S., Fung, I. Y., Liu, Y., & Chiang, J. C. H. (2014). Remote Vegetation Feedbacks
1146 and the Mid-Holocene Green Sahara. *Journal of Climate*, 27(13), 4857–4870.
1147 <https://doi.org/10.1175/JCLI-D-13-00690.1>
- 1148 Tabor, C., Otto-Bliesner, B., & Liu, Z. (2020). Speleothems of South American and Asian
1149 Monsoons Influenced by a Green Sahara. *Geophysical Research Letters*, 47(22),
1150 e2020GL089695. <https://doi.org/https://doi.org/10.1029/2020GL089695>
- 1151 Tarnocai, C. (1990). Paleosols of the Interglacial Climates in Canada. *Géographie Physique et*
1152 *Quaternaire*, 44(3), 363–374. <https://doi.org/https://doi.org/10.7202/032836ar>
- 1153 Teed, R. (2000). A >130,000-Year-Long Pollen Record from Pittsburg Basin, Illinois.
1154 *Quaternary Research*, 54(2), 264–274.
1155 <https://doi.org/https://doi.org/10.1006/qres.2000.2161>
- 1156 Thompson, A. J., Zhu, J., Poulsen, C. J., Tierney, J. E., & Skinner, C. B. (2022). Northern
1157 Hemisphere vegetation change drives a Holocene thermal maximum. *Science Advances*,
1158 8(15), eabj6535. <https://doi.org/10.1126/sciadv.abj6535>
- 1159 Thompson, R., Whitlock, C., Bartlein, P., & Al., E. (1993). Climatic Changes in the Western
1160 United States since 18,000 yr B.P. In H. Wright, J. Kutzbackm, I. Webb, T, W. Ruddiman,
1161 S.-P. FA, & P. Bartlein (Eds.), *Global Climates Since the Last Glacial Maximum* (pp. 468–
1162 513). University of Minnesota Press.
- 1163 Tierney, J. E., Poulsen, C. J., Montañez, I. P., Bhattacharya, T., Feng, R., Ford, H. L., Hönisch,
1164 B., Inglis, G. N., Petersen, S. V, Sagoo, N., Tabor, C. R., Thirumalai, K., Zhu, J., Burls, N.
1165 J., Foster, G. L., Goddérus, Y., Huber, B. T., Ivany, L. C., Turner, S. K., ... Zhang, Y. G.
1166 (2020). Past climates inform our future. *Science*, 370(6517), eaay3701.
1167 <https://doi.org/10.1126/science.aay3701>
- 1168 Tingstad, A., Groves, D., & Lempert, R. (2014). Paleoclimate Scenarios to Inform Decision
1169 Making in Water Resource Management: Example from Southern California's Inland
1170 Empire. *Journal of Water Resources Planning and Management*, 140, 4014025.
1171 [https://doi.org/10.1061/\(ASCE\)WR.1943-5452.0000403](https://doi.org/10.1061/(ASCE)WR.1943-5452.0000403)
- 1172 Trenberth, K. E. (2011). Changes in precipitation with climate change. *Climate Research*, 47(1–
1173 2), 123–138. <https://doi.org/10.3354/cr00953>
- 1174 Whitlock, C., & Bartlein, P. J. (1997). Vegetation and climate change in northwest America
1175 during the past 125 kyr. *Nature*, 388(6637), 57–61. <https://doi.org/10.1038/40380>
- 1176 Wise, E. K. (2016). Five centuries of U.S. West Coast drought: Occurrence, spatial distribution,
1177 and associated atmospheric circulation patterns. *Geophysical Research Letters*, 43(9),
1178 4539–4546. <https://doi.org/10.1002/2016GL068487>
- 1179
1180

- 1181 Wong, C. I., Potter, G. L., Montañez, I. P., Otto-Bliesner, B. L., Behling, P., & Oster, J. L.
1182 (2016). Evolution of moisture transport to the western U.S. during the last deglaciation.
1183 *Geophysical Research Letters*, 43(7), 3468–3477.
1184 <https://doi.org/https://doi.org/10.1002/2016GL068389>
- 1185 Woodhouse, C., Lukas, J., Morino, K., Meko, D., & Hirschboeck, K. (2016). *Using the Past to*
1186 *Plan for the Future—The Value of Paleoclimate Reconstructions for Water Resource*
1187 *Planning* (pp. 161–182). <https://doi.org/10.1201/b19534-12>
- 1188 Woolfenden, W. B. (2003). A 180,000-year pollen record from Owens Lake, CA: terrestrial
1189 vegetation change on orbital scales. *Quaternary Research*, 59(3), 430–444.
1190 [https://doi.org/https://doi.org/10.1016/S0033-5894\(03\)00033-4](https://doi.org/https://doi.org/10.1016/S0033-5894(03)00033-4)
- 1191 Wyatt, P. (1990). Amino Acid Evidence Indicating Two or More Ages of Pre-Holocene
1192 Nonglacial Deposits In Hudson Bay Lowland, Northern Ontario. *Géographie Physique et*
1193 *Quaternaire*, 44(3), 389–393. <https://doi.org/https://doi.org/10.7202/032838ar>
- 1194